

Dark matter candidates

GRAPPA seminar

Rose Grey, Gabriël Koole, Davey Oogjes and Samuel van Beek

June 29, 2018

Abstract

In this review article we give an overview of popular dark matter candidates. The properties and production mechanism of weakly interacting massive particle (WIMPs) such as neutralinos in supersymmetry models and the lightest Kaluza-Klein particle (LKP) in models of universal extra dimensions are discussed. Also, we give an overview of the different non-WIMPs sterile neutrinos, axions, fuzzy dark matter and WIMPzillas. Finally, special attention is given to primordial black holes (PBHs) as a dark matter candidate. For all candidates we give a brief theoretical motivation and discuss current constraints from observations.



UNIVERSITEIT VAN AMSTERDAM



Contents

1	Introduction (Gabriël)	3
2	WIMPs	4
2.1	Properties of WIMPs (Rose)	4
2.2	The freeze out mechanism (Gabriël)	5
2.3	SUSY (Samuel)	8
2.3.1	The neutralino	8
2.3.2	Neutralino production and annihilation	9
2.3.3	Interactions involving neutralinos	10
2.4	Universal Extra Dimension (Rose)	11
2.5	Constraints from collider experiments (Davey)	13
3	Non-WIMPs	14
3.1	Sterile neutrinos (Gabriël)	14
3.1.1	Motivation for sterile neutrinos	14
3.1.2	Production in the early Universe	15
3.1.3	Searches for DM sterile neutrinos	17
3.2	Axions (Samuel)	18
3.2.1	Strong CP problem	18
3.2.2	The Peccei-Quinn solution	19
3.2.3	Axions as dark matter candidates	19
3.2.4	Experimental searches for axions	20
3.3	Fuzzy Dark Matter (Rose)	21
3.3.1	Light Spin Zero Fields	23
3.3.2	Astrophysical Consequences	24
3.3.3	Final remarks	26
3.4	WIMPzillas (Davey)	26
3.4.1	WIMPzilla properties	27
3.4.2	WIMPzilla production	27
3.4.3	The GZK-limit and WIMPzillas	28
4	Primordial Black Holes	28
4.1	Motivation for Primordial Black Holes (Rose)	28
4.2	PBH Capture (Rose)	29
4.3	The merger rate of PBH binaries (Gabriël)	33
4.3.1	Did LIGO detect dark matter?	33
4.3.2	The close encounter scenario	33
4.3.3	PBH binary formation in the early Universe	34
4.4	Gravitational lensing (Samuel)	36
4.4.1	Strong lensing	37
4.4.2	Microlensing	37
4.4.3	Weak lensing	38
4.4.4	Femtolensing	39
4.4.5	More results for dark matter	39
4.5	Constraints from X-ray / Radio (Davey)	39

1 Introduction (Gabriël)

One of the most important problems in particle physics and cosmology is the nature of dark matter (DM) in the Universe. Evidence for the existence of large amounts of DM in the Universe has been increasing steadily over last decades, yet its origin and nature remain unknown at this time.

A popular view on dark matter is that it consists of weakly interacting massive particles (WIMPs). This is a popular DM candidate for a number of reasons. First of all, in many theoretically well-motivated extensions of the Standard Model (SM) WIMPs arise naturally. In addition, WIMPs are attractive experimentally because their detection rates are within reach of current or future detectors [1]. The third and perhaps most enticing feature of WIMPs as a DM candidate is that the production mechanism of the DM abundance today, the *thermal freeze out* mechanism, is simple and understood entirely [2]. The freeze out mechanism will be discussed in section 2.2. The beauty of this mechanism is emphasised by the so-called the *WIMP miracle*. To account for the amount of DM in the Universe today, the freeze out mechanism provides constraints on the mass and the cross section of the WIMP. Using the observed DM abundance today, a particle with a mass in the range of tens-hundreds GeV and a cross section which corresponds to weak interaction is predicted [3]. These properties coincide with the expected properties of the lightest stable particle (LSP) in many supersymmetric (SUSY) models. An LSP like the lightest neutralino \tilde{X}_1^0 is therefore an excellent WIMP candidate [4]. The seemingly magical correlation between the DM problem and SUSY models, which were initially proposed as a solution to the hierarchy problem in the SM, is therefore named the WIMP miracle. The properties of the lightest neutralino as a DM candidate will be discussed in section 2.3.

Besides the neutralino in SUSY models, other beyond the Standard Model (BSM) theories provide other WIMP candidates. One of these theories suggests the existence of an extra spatial dimension. This extra dimension takes several forms, but this review focuses on the DM candidate coming from a universal extra dimension (UED). In UED the 5-dimensional spacetime is reduced to the 4-dimensional spacetime using the Kaluza-Klein (KK) method. It was initially motivated to unify electromagnetism with gravity, although it has had influence in many other fields of physics. The DM candidate that arises in these models is known as the lightest Kaluza-Klein particle (LKP). See section 2.4 for a more detailed discussion of UED.

Although WIMPs are a very popular DM candidate, conclusive evidence has not been discovered yet. Therefore alternative theories on DM remain relevant. In this paper we discuss a number of popular non-WIMPs from very light axions to extremely heavy WIMPzillas. These DM candidates were not necessarily produced in a thermal freeze out as WIMPs were, but via different production mechanisms. In section 3 these candidates are discussed.

Since the first detection of gravitational waves from the merger of a black hole binary by the LIGO and VIRGO collaborations [5], another non-WIMP DM candidate received a lot of attention: primordial black holes (PBHs) (see [6]). These black holes were formed in the early Universe and could potentially explain DM. The reason that PBHs as DM candidate rekindled is that the masses of the black holes in the LIGO/VIRGO gravitational wave detection fall precisely in the mass window that was not excluded by other constraints. Section 4 discusses the properties and

current constraints on PBH DM.

This review is organized as follows. In section 2 WIMPs are discussed starting with the general properties (2.1), followed by the freeze out mechanism (2.2), WIMPs in supersymmetric (SUSY) models (2.3), the LKP in universal extra dimension models (2.4) and constraints on WIMPs from collider searches (2.5). Section 3 gives an overview of the popular non-WIMPs: sterile neutrinos (3.1), axions (3.2), fuzzy dark matter (3.3) and WIMPzillas (3.4). The entire section 4 is devoted to discuss the properties of PBHs (4.1) and the constraints from captures by stars (4.2), the merger rate of PBH binaries (4.3), gravitational lensing (4.4) and X-ray/Radio radiation (4.5).

2 WIMPs

2.1 Properties of WIMPs (Rose)

As DM constitutes $\sim 85\%$ of the matter in our universe, a pressing question to ask ourselves: what is DM actually made of? Through observations, various properties of these particles have been deduced, which leads us to rule out a family of candidates. However, there is still a large number of possible candidates, with masses ranging from 10^{-5} eV to $10^4 M_\odot$ [7]. One particular model is known as WIMPs. This has properties as follows:

- *Massive.*

Their effects were historically noticed when the calculation of the angular momentum of the galaxy was smaller than the observed result. This is because the calculations used a mass approximation from all observable stars, with an average estimation for the bodies orbiting them. It was concluded that there must be matter we cannot see, hence the terminology Dark Matter. It is considered to reside in a halo around the galaxy. Generally, they are said to have masses in the range of $10 \text{ GeV} \sim 1 \text{ TeV}$ [7].

- *Cold.*

Here the term cold means non-relativistic. DM has also been attributing some contribution towards structure formation, where massive non-relativistic particles will allow structure to form hierarchically [8]. DM will cause small particles to gravitationally collapse, which in turn will pull more and more objects until large-scale structures are formed. The theory for cold DM has been solidified due to advancements with the Lambda-CDM model [9].

- *Non-baryonic.*

The root cause for the non-baryonic property is still an ongoing investigation in DM physics. Measurements for the current energy density of baryonic matter has almost all of the baryonic matter accounted for in luminous objects. The measurement of this density combines some of the most precise measurements in modern cosmology¹. There is a large deficit for an explanation for non-

¹ From BBN, we have a measurement of the baryonic density up to a 95% confidence level [10]. There is a single value of baryon-photon ratio that accounts for the observed abundances of light elements. The number of photons is also a well documented number from the CMB [11].

baryonic objects in luminous matter [12]. This also leads us to believe that our non-luminous matter is non-baryonic.

- *Weakly Interacting.*

Constraints have been put on the WIMP cross-section, roughly in the range of $10^{-28} - 10^{-23}$ [13]. Combining this with the mass constraint, this is the behaviour we would expect from a weakly interacting particle.

- *Electrically Neutral.*

This is synonymous with being dark. If they are not electrically neutral, they would interact with photons and emit light that we would be able to detect.

- *Stable.*

It should go without saying any DM particle must be stable. We assume that DM has been around since the beginning of time, having a similar abundance as that of the abundance at the time of its freeze-out. If these particles could decay, they would have all decayed after ~ 14 billion years, and their effects would not be visible today.

The above properties describe a family of candidates known as WIMPs. Although the finer details of these particles will be different from model to model, these basic properties have been well implemented. They are a new fundamental particle and are an addition to the SM. Some basic models are particles arising from supersymmetry and a universal extra dimension, as well as a particle known as the Little Higgs [14].

2.2 The freeze out mechanism (Gabriël)

As briefly mentioned in the introduction the freeze out mechanism is the production mechanism of the WIMP DM abundance today. In the early Universe the WIMP, denoted as X , and the SM particles were in close contact at high temperatures ($T \gg m_X$). The cosmological plasma (containing the SM particles) and the DM were in thermal equilibrium due to DM particle production from annihilations [1]. The annihilation rate is given by $\Gamma_{\text{ann}} = n_X \langle \sigma_{\text{ann}} v \rangle$ where n_X is the number density of DM particles, and $\langle \sigma_{\text{ann}} v \rangle$ thermally averaged product of the annihilation cross section and the velocity [15]. A freeze out is defined as the inability of annihilations to keep the particle in thermal equilibrium [16]. The freeze out, or thermal decoupling, of DM occurred when the annihilation rate became smaller than the expansion rate of the Universe $\Gamma_{\text{ann}} \lesssim H$. In other words, the DM particles were being separated by the expansion of the Universe faster than they could annihilate to maintain equilibrium, resulting in a freeze out and a relic density of DM WIMPs. Using this mechanism we can calculate this relic density of DM.

We start with the Boltzmann equation for the DM number density n_X and the law of entropy conservation:

$$\frac{dn_X}{dt} = -3Hn_X - \langle \sigma_{\text{ann}} v \rangle \{n_X - n_X^{(0)}\}, \quad (1)$$

$$\frac{ds}{dt} = -3Hs, \quad (2)$$

where t is time, s is the entropy density, H is the Hubble constant, and $n_X^{(0)}$ is the equilibrium density [17]. Eq. 1 and 2 can be combined into a single equation. Defining $Y \equiv n_X/s = n_X/T^3$, the WIMP yield, the Boltzmann equation for a DM particle becomes:

$$\frac{dY}{dt} = T^3 \langle \sigma_{\text{ann}} v \rangle \{ Y_{\text{EQ}}^2 - Y^2 \}, \quad (3)$$

where $Y_{\text{EQ}} = n_X^{(0)}/T^3$ [16]. In the literature this equation is often rewritten in terms of a new variable $x \equiv m_X/T$ for convenience. Eq. 3 then becomes:

$$\begin{aligned} \frac{dY}{dx} &= \frac{1}{3H} \frac{ds}{dx} \{ Y^2 - Y_{\text{EQ}}^2 \} \\ &= -\frac{\lambda}{x^2} \{ Y^2 - Y_{\text{EQ}}^2 \}. \end{aligned} \quad (4)$$

Here, λ is the ratio of the annihilation rate to the expansion rate:

$$\lambda \equiv \frac{m_X^3 \langle \sigma_{\text{ann}} v \rangle}{H(m_X)}, \quad (5)$$

where $H(m_X) = Hx^2$ in the radiation era where dark matter production typically occurs [16]. Since the DM particles are relativistic in this era, $x \gg 1$, the equilibrium abundance Y_{EQ} will exponentially suppressed. Therefore Eq. 4 simplifies to:

$$\frac{dY}{dx} \simeq -\frac{\lambda Y^2}{x^2}. \quad (6)$$

Integrating this from the freeze out (Y_{fo}) to late times (Y_∞) and using the fact that typically $Y_{\text{fo}} \gg Y_\infty$, the DM abundance today becomes $Y_\infty \simeq x_{\text{fo}}/\lambda$. The number density at late times is $Y_\infty T^3$, so the energy density of DM today can be expressed as:

$$\rho_X = m_X Y_\infty T^3 \simeq \frac{m_X Y_\infty T_0^3}{30}, \quad (7)$$

where T_0 is the temperature today [16]. Using the expression for Y_∞ , the DM abundance $\Omega_X h^2$ can be derived:

$$\begin{aligned} \Omega_X h^2 &\equiv \frac{\rho_X h^2}{\rho_c} = \frac{m_X Y_\infty T_0^3 h^2}{30 \rho_c} \\ &= \frac{x_{\text{fo}}}{\lambda} \frac{m_X T_0^3 h^2}{30 \rho_c} \\ &= \frac{x_{\text{fo}}}{m_X^2 \langle \sigma_{\text{ann}} v \rangle} \frac{T_0^3 h^2 H(m_X)}{30 \rho_c}. \end{aligned} \quad (8)$$

where ρ_c is the critical density. Finally the Hubble rate at freeze out $H(m_X)$ can be calculated (see [16]) and the quantities $T_0 \simeq 2.35 \times 10^{-13}$ GeV and $\rho_c \simeq 8 \times 10^{-47} h^2$ GeV⁴ are known [1]. Jungman et al. [7] estimated the relic density to be

$$\Omega_X h^2 = \frac{3 \times 10^{27} \text{cm}^3 \text{s}^{-1}}{\langle \sigma_{\text{ann}} v \rangle}. \quad (9)$$

Eq. 9 can be applied for any kind of cold DM to find the minimal mass for a typical WIMP. Using this, Lee and Weinberg [18] first concluded that a WIMP with $m \lesssim 2$ GeV is precluded. This lower mass bound for WIMPs is therefore known as the Lee-Weinberg bound. The upper limit on the WIMP mass is set by the so-called unitarity bound. Griest and Kamionkowski [19] applied this bound to derive an upper limit on the DM particle mass:

$$m_X \lesssim 340 \text{ TeV}. \quad (10)$$

It is now possible to find the value of $\langle\sigma_{\text{ann}}v\rangle$ for a given WIMP mass for which $\Omega_X h^2$ is in agreement with the measured value $\Omega_{\text{CDM}} h^2 = 0.1120 \pm 0.0056$ [20]. Figure 1 shows the abundance of the WIMP versus x . For the weak interaction cross-section, $\langle\sigma_{\text{ann}}v\rangle = 2 \times 10^{-26} \text{ cm}^3 \text{s}^{-1}$, the relic density is compatible with observations. Since this cross-section and mass range coincide with the properties of the lightest supersymmetric particle in many SUSY models, this is often called the WIMP miracle. DM candidates from SUSY models will be discussed in the next section.

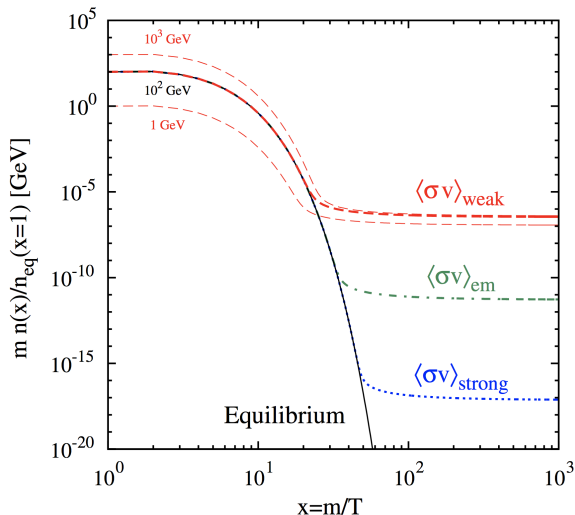


Figure 1: Evolution of the cosmological WIMP abundance as a function of $x = m/T$. Note that the y axis spans 25 orders of magnitude. The thick curves show the WIMP mass density, normalised to the initial equilibrium number density, for different choices of annihilation cross section $\langle\sigma_{\text{ann}}v\rangle$ and mass m . Results for $m = 100$ GeV are shown for weak interactions, $\langle\sigma_{\text{ann}}v\rangle = 2 \times 10^{-26} \text{ cm}^3 \text{s}^{-1}$, (dashed red), electromagnetic interactions, $\langle\sigma_{\text{ann}}v\rangle = 2 \times 10^{-21} \text{ cm}^3 \text{s}^{-1}$ (dot-dashed green), and strong interactions, $\langle\sigma_{\text{ann}}v\rangle = 2 \times 10^{-15} \text{ cm}^3 \text{s}^{-1}$ (dotted blue). For the weak cross section the thin dashed curves show the WIMP mass dependence for $m = 10^3$ GeV (upper dashed curve) and $m = 1$ GeV (lower dashed curve). The solid black curve shows the evolution of the equilibrium abundance for $m = 100$ GeV. Figure taken from [20].

2.3 SUSY (Samuel)

In many theories for physics beyond the Standard Model, supersymmetry is an important feature. One problem in particle physics is the hierarchy problem. Instead of extraordinary fine tuning by means of quantum corrections regarding the electroweak scale and the Planck scale, supersymmetry solves the hierarchy problem naturally by introducing superpartner particles through which the quantum corrections are cancelled. However, SUSY is not only a solution to the hierarchy problem. Supersymmetry could provide answers on the nature of dark matter in the sense that a combination of supersymmetric transformations leads to a spacetime transformation. Subsequently, theories of local supersymmetry necessarily contain local spacetime transformations and thus contain gravity [7]. Dark matter is subject to gravitational forces and therefore supersymmetry is an interesting study area to investigate dark matter.

One important ingredient in supersymmetric dark matter is R -parity. This discrete symmetry can be written as $R = (-1)^{3(B-L)+2S}$. Here, B is the baryon number, L the lepton number and S the spin. Regarding SM particles, $R = 1$ and for supersymmetric partner particles $R = -1$. In case of R -parity violation, no selection rules exist that would prevent the decay of the supersymmetric particles to particles of the order of a few GeV. However, no stable supersymmetric particles could exist if all these particles decay. Therefore, only supersymmetry with invariant R -parity is considered. This provides a lightest R -odd particle that is stable and does not decay to other SM or SUSY particles. This particular particle is called the lightest supersymmetric particle (LSP).

In the minimal supersymmetric extension of the Standard Model, there is a successful gauge coupling unification. The term *minimal* refers to the limit on the superpartner masses of a few TeV [21], which is already quite heavy compared to Standard Model particles. The extension consists of adding supersymmetric partners that corresponds to the fields of the Higgs doublet extension in the Standard Model [22]. A Standard Model particle together with its corresponding superpartner together form a supermultiplet. In Table 1 the MSSM particles are listed together with their quantum numbers.

The superpartners of the W-boson and the charged Higgs bosons are the charged higgsino and gaugino. The same $SU(3) \times U(1)$ quantum numbers are associated with the supersymmetric particles. Hence, mixing will occur after electroweak-symmetry breaking. Linear combinations provide mass eigenstates that are known as *charginos* (χ_1^\pm). In particular, the superpartners of the photon, the Z-boson and the neutral Higgs boson (the photino, zino and neutral higgsino, respectively) generally mix into four mass eigenstates called *neutralinos* ($\chi_1^0, \chi_2^0, \chi_3^0, \chi_4^0$). The lightest of these four supersymmetric particles, χ_1^0 , would be the LSP in the MSSM and weakly interacting. Therefore the neutralino is a considerable dark matter-candidate. The other neutralinos and the charginos may decay into the lightest neutralino.

2.3.1 The neutralino

The mass eigenstate of the neutralino can be written as a linear combination of neutral higgsinos, the wino and the bino [7]. The bino is a $U(1)$ superpartner of the corresponding to weak hypercharge. It is the lightest gaugino [23], a superpartner of a gauge field.

Table 1: Overview of the fields in the MSSM together with the associated $SU(3) \otimes SU(2) \otimes U(1)$ quantum numbers. Only the first generation of particles is considered regarding quarks and leptons [22].

Field Content of the MSSM						
Super-multiplets	Super-field	Bosonic fields	Fermionic partners	SU(3)	SU(2)	U(1)
gluon/gluino	\widehat{V}_8	g	\tilde{g}	8	1	0
gauge/ gaugino	\widehat{V} \widehat{V}'	W^\pm, W^0 B	$\widetilde{W}^\pm, \widetilde{W}^0$ \widetilde{B}	1 1	3 1	0 0
slepton/ lepton	\widehat{L} \widehat{E}^c	$(\tilde{\nu}_L, \tilde{e}_L^-)$ \tilde{e}_R^-	$(\nu, e^-)_L$ e_R^-	1 1	2 1	-1 -2
squark/ quark	\widehat{Q} \widehat{U}^c \widehat{D}^c	$(\tilde{u}_L, \tilde{d}_L)$ \tilde{u}_R \tilde{d}_R	$(u, d)_L$ u_R d_R	3 3 3	2 1 1	1/3 4/3 -2/3
Higgs/ higgsino	\widehat{H}_d \widehat{H}_u	(H_d^0, H_d^-) (H_u^+, H_u^0)	$(\tilde{H}_d^0, \tilde{H}_d^-)$ $(\tilde{H}_u^+, \tilde{H}_u^0)$	1 1	2 2	-1 1

$$\tilde{\chi}^0 = N_{10}\tilde{B} + N_{20}\tilde{W}^3 + N_{30}\tilde{H}_1^0 + N_{40}\tilde{H}_2^0 \quad (11)$$

Here, N_{i0} are coefficients that are determined by diagonalization of the mass matrix of the neutralino. The subscript 0 denotes that the lightest of the four possible neutralinos is considered. $\tilde{B}, \tilde{W}^3, \tilde{H}_i^0$ are the superpartners mentioned above.

2.3.2 Neutralino production and annihilation

The simplest process for neutralino production is through electron-positron annihilation resulting in a neutralino pair via the Z^0 resonance. Neutralinos can annihilate into many final states. The most important states are the states that are present in lowest order perturbation theory. Possible states are fermion-antifermion pairs and combinations of the W-bosons, Z-boson or Higgs bosons. To study the neutralinos, the annihilation cross-section in the non-relativistic case is needed. The cross-section σ_A can be written as

$$\sigma_A v = a + b v^2 + \mathcal{O}(v^4) \quad (12)$$

The term a comes from s -wave annihilation if velocity v is zero and the term $b v^2$ comes from both s - and p -wave annihilation [24]. For s -waves, the angular momentum $l = 0$. For p -waves, $l = 1$. If s -wave contribution is not suppressed and $\langle \sigma_A v \rangle$ is energy independent, only a is needed. However, s -wave annihilation into light fermions could be suppressed due to helicity considerations. Therefore, $b v^2$ needs to be incorporated as well.

For the relic abundance of dark matter the following formula is used [24].

$$\Omega h^2 \approx 2.82 \times 10^8 Y_\infty(m_\chi/\text{GeV}) \quad (13)$$

with

$$Y_\infty^{-1} = 0.264 g_*^{1/2} m_{Pl} m_\chi (a/x_f + 3(b - a/4)/x_f^2) \quad (14)$$

The epoch of freezout is determined by

$$x_f = \ln[0.0764 m_{Pl} (a + 6b/x_f) \kappa (2 + \kappa) m_\chi / (g_* x_f)^{1/2}] \quad (15)$$

Here, κ is a constant of order unity that is tuned to match the late- and early-time solutions. In short, if $a \gg b$, then $\langle \sigma_A v \rangle = a$. If $a \ll b$, then $\langle \sigma_A v \rangle \approx 6b/x_f$, with $x_f = T_f/m_\chi$, which is the case at freezeout [7]. Therefore, both a and b are needed for calculations. For all possible decay product of the neutralino, the a and b contributions have been calculated [7].

During the freeze-out, the neutralinos moved with speeds around $0.5c$. However, at low energies, the scattering amplitudes of particles are independent of the angle. Neutralinos in the galaxy move relatively slow $\sim 0.001c$ [7], meaning that only a is needed for calculations regarding relic neutralinos.

As an interaction example, the neutralino could annihilate to weak gauge bosons when the mass is high enough, i.e. $m_\chi > m_W$. It was found that annihilation to a W/Z -boson pair is not subject to s -wave suppressions mechanisms, making neutralinos important for these pair productions in case the neutralinos are heavy enough [25]. Multiple annihilation processes are possible regarding W/Z -bosons. In Figures 2 and 3 the Feynman diagrams for these processes are shown.

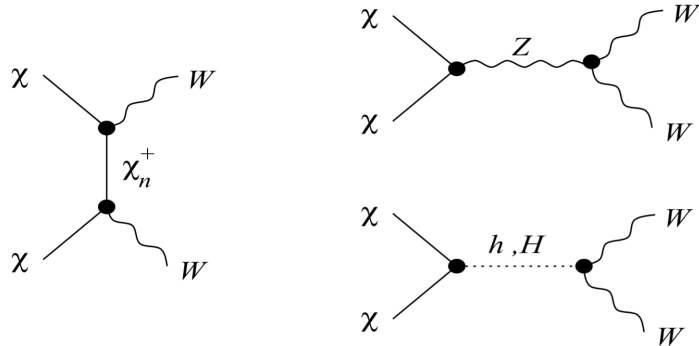


Figure 2: Feynman diagrams for neutralino annihilation and W -boson pair creation via chargino, Z -boson or Higgs boson [7]

Similar processes are found for the other final states. Many channels are closed or suppressed due to too light neutralino masses. Therefore, fermionic final states are often the channels that are open.

2.3.3 Interactions involving neutralinos

Neutralinos do not have vector interactions with other particles, since neutralinos are Majorana fermions (neutralino is its own anti-particle) [7]. Therefore, only spin-spin interactions and scalar interactions are considered. The total elastic-scattering cross-section is the sum of the two types of interaction of the neutralino.

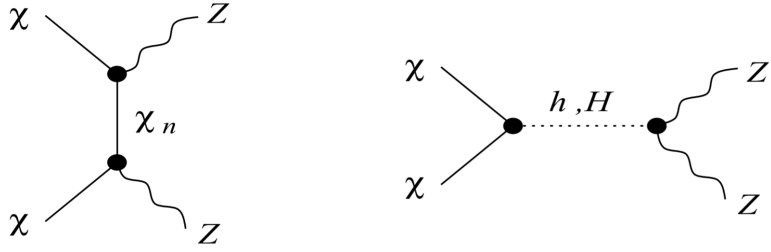


Figure 3: Feynman diagrams for neutralino annihilation and Z-boson pair creation, via neutralino or Higgs boson

The spin interaction of a neutralino with another particle's spin is an axial-vector interaction. The scalar interaction is between the mass of the neutralino and a nucleon's mass.

2.4 Universal Extra Dimension (Rose)

Although the neutralino is a strong candidate as a DM particle, while the identity of the DM particle remains unknown we will also probe alternative theories. One of these theories is the existence of an extra spatial dimension. This spatial dimension would arise at a high energy scale. The idea is motivated by string theory and M-Theory. Although these will not be discussed at length in this review; an excellent reference for this would be [26].

This has multiple benefits to the standard model, including anomaly cancellation, dynamical electroweak symmetry breaking, prevention of rapid proton decay and, for the importance of this review, a DM candidate [27]. This extra dimension takes several forms. Firstly there is a universal extra dimension (UED) [28], in which all particles in the Standard Model will propagate on. Alternatively, our observable (3+1) dimensional space is a brane existing in a higher (3+ δ +1) bulk spacetime [29]. In the Arkani-Hamed, Dimopoulos and Dvali (ADD) model, all Standard Model particles will propagate on 3 spatial dimensions whereas the graviton will propagate in the bulk. There are also intermediate theories, where only certain families will propagate in the bulk, which gives rise to the anomaly cancellations [30]. We could also consider a warped extra dimension, a dimension with a non-factorisable, 'warped', geometry [31]. The DM candidate comes from UED, and therefore for the remainder of this review we shall be focusing on UED.

UED offers an additional feature not seen in the brane approach. There remains translational symmetry, leading to a conservation of the momentum in all dimensions. In UED, the extra spatial dimension is flat space compactified onto S^1 . The method used to reduce the 5-dimensional theory to the 4-dimensional one is known as Kaluza Klein (KK) reduction, which gives a number of interesting properties. We will give a brief, simplified description of origin of KK modes shortly. To account for chiral fermions, a Z_2 symmetry needs to be imposed, i.e. $x^4 \rightarrow -x^4$. Fields can be even or odd under this symmetry. The compactified space is therefore known as an S^1/Z_2 orbifold [32]. We will have orbifold fixed points at $x^4 = 0, \pi R$. These fixed points will break translational symmetry in the x^5 direction, also breaking momentum conservation. A symmetry known as the KK number, coming from momentum conservation, is therefore also broken by this Z_2 symmetry. But a residual conserva-

tion is seen; the KK-parity is given by $(-1)^m$. All modes with odd m will be charged under this parity. It will be clear there will be mixing between KK modes due to this broken momentum conservation. The DM candidate emerging from these modes is known as the lightest Kaluza-Klein particle (LKP), where $m = 1$ [33]. It was first discussed by Kolb and Slansky, who coined it the pyrgons [34]. The LKP is stable as it is protected by KK-parity, at tree-level, with all other KK particles decaying into the LKP. As stated, a DM candidate must be stable, electrically neutral and non-baryonic. The best candidates from this theory then become the first level KK modes of the neutral gauge bosons (the photon and Z boson) and the neutrino. Following the notation of [33], we will refer to the first photon mode as $B^{(1)}$.

Returning to the KK modes, first consider imposing periodic boundary conditions on our orbifold (we consider fields even under Z_2), expanding in Fourier modes gives us particles in the form (suppressing spacetime indices),

$$\psi(x^\mu, x^4) = \sum_{n \in \mathbf{Z}} e^{(inx^4/R)} \phi_n(x^\mu) \quad (16)$$

where the quantisation of the momentum in the extra dimension, x^4 , keeps the wavefunction single-valued [35]. Here R is the radius of the orbifold. For completeness, $\phi_n^* = \phi_{-n}$. Using the equation of motion, it can be seen that there are mass modes of $M_n^2 \sim M_0^2 + n^2/R^2$, where M_0 is the mass as seen in the Lagrangian. We have found the infinite tower of KK modes. The other quantum numbers of the particle will remain unchanged. The zero modes here correspond to Standard Model states [32]. A detection of the higher modes, as seen by CERN, would appear as periodic spikes in the number of events as a function of centre of mass energy. So far no such signal has been found.

The relic density of $B^{(1)}$ has been computed in [33], where they considered coannihilations with the next lightest KK particle, $e_R^{(1)}$, the right handed first KK mode of the electron. It can be seen in Figure 4. It was assumed all other modes are too heavy to contribute. The relative mass difference between the LKP and the NLKP was inputted as

$$\Delta = \frac{m_{NLKP} - m_{LKP}}{m_{LKP}} \quad (17)$$

It is important to note that the density of the $B^{(1)}$ is increased when considering $e_R^{(1)}$ than without. This is because the cross section for self-annihilation is larger than the cross-section for coannihilation; the particles will decouple at a similar time with coannihilation as without, and the remaining $e_R^{(1)}$ will decay into $B^{(1)}$. The green region is the required relic density, which corresponds to masses between 0.6 – 1.2 TeV depending on the model considered.

The first mode of the neutrino, $\nu^{(1)}$ has also been considered as a possible candidate. It satisfies stable, electrically neutral and non-baryonic conditions required from WIMPs. Its relic density has been discussed in further detail in [33].

There are other nuances to consider with these particles, these have been discussed in other papers at length. We have used mostly tree-level consideration, but for a paper on the radiative correction to the mass of the KK particles, see [36]. They consider the fact that the extra dimensions in our theory will violate Lorentz symmetry, giving corrections to the mass beyond tree-level. We would also stumble upon log divergences and interactions between only even or odd KK modes. Further

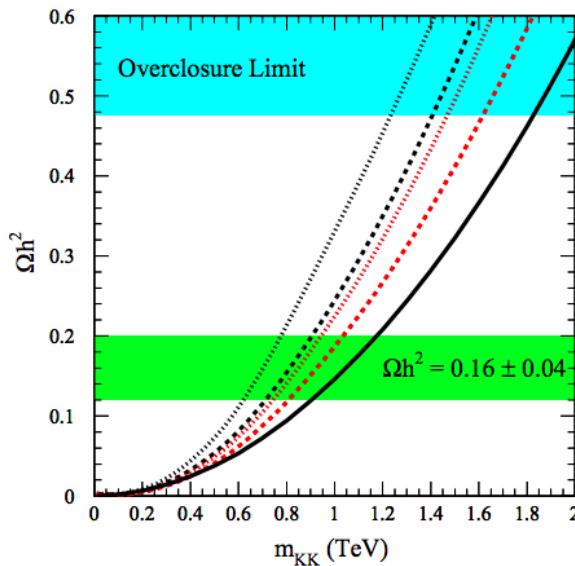


Figure 4: The relic density of $B^{(1)}$ against its mass. The solid line considers $B^{(1)}$ alone, and the dashed and dotted lines correspond to the case in which there are one or three flavors of nearly degenerate $e^{(1)}$ respectively. For each case, the black curves denote the case $\Delta = 0.01$ and the red curves $\Delta = 0.05$. Figure taken from [33].

discussion on direct detection can be found in [37]. Recent experimental bounds on R are given by $R \lesssim 40 \mu\text{m}$ [38].

2.5 Constraints from collider experiments (Davey)

As WIMPs interact very weakly with normal matter, one would assume that trying to find them using high energy particle colliders is unfeasible. However, finding indications of dark matter is one of the big aims of the LHC. Although dark matter most likely can not be directly detected in a collision experiment, it *is* possible to see the effects of dark matter. As the direct WIMP searches depend on a coupling of WIMPs to nucleons, it is expected for WIMPs that they will also be produced in high energy hadron-hadron collisions. In proton-proton collisions transverse momentum p_T and transverse energy E_T , transverse meaning perpendicular to the beam line, need to be conserved. As nowadays the standard model and experimental background are well understood, it is possible to reconstruct the collision from the data, and thus to find indications of dark matter in the form of missing transverse energy and momentum. Applying a multitude of dark matter models to these possible signatures then in turn constrains the parameter space of these models, which can narrow the search range for direct and indirect detection experiments and also rule out possible signals *from* these experiments.[39] An example of this can be found in [40], where the constrained Minimal Supersymmetric Standard Model(cMSSM) is ruled out using observational data and experimental data from the LHC.

In the case of SUSY, which is thought to be the most natural extension to the Standard Model, 105 new parameters are added to the SM, which are far too many to be able to make any significant constraints. For this reason the models are sim-

plified greatly until only a few parameters remain. Creating random values for these parameters and then fitting them to ATLAS data rules out a lot of models already, an example of which is shown in fig 5, where the density of allowed phenomenological MSSM models in the plane of dark matter relic density versus the LSP mass is shown before and after the results of 22 separate ATLAS searches are combined to constrain the parameter space of this model.

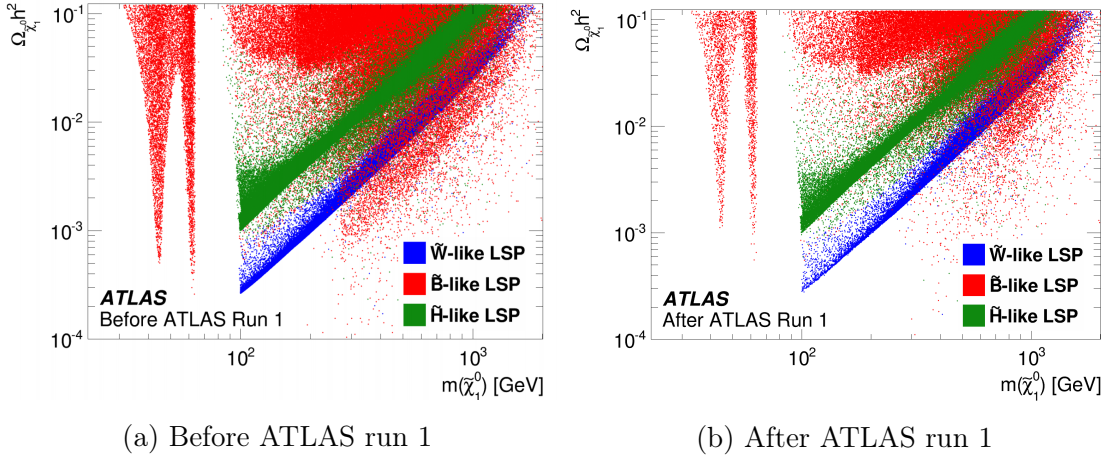


Figure 5: The density of pMSSM models for dark matter relic density versus LSP mass, before and after constraints from ATLAS results. Taken from [41].

While the previous example was for a specific UV-complete theory, constraints from colliders can also be applied in a more generic way. By taking a very simplified model of a dark matter particle interacting with SM particles through a mediator, constraints can be put on the mass of the DM particle and the mediator without taking account any model specific parameters. An example of this is shown in fig 6.

3 Non-WIMPs

3.1 Sterile neutrinos (Gabriël)

3.1.1 Motivation for sterile neutrinos

Neutrinos are the only electrically neutral, long-lived particles in the Standard Model. The discovery of neutrino oscillations [43, 44] proved that neutrinos have mass. It was therefore widely thought that neutrinos would make up DM. A background of DM neutrinos would be created by means of a freeze out, exactly as discussed in section 2.2. In order for neutrinos to play the role of DM, the sum of the masses of all neutrino flavours should be about 11.5 eV [45]. This is clearly not the case, as it is in conflict with experimental results. The sum of neutrino masses has been determined to be below 2 eV in β -decay experiments [46] while cosmological data provides an upper bound of 1.3 eV at 95% CL [47]. Another constraint comes from the fact that neutrinos are fermions. Due to the Pauli exclusion principle, the phase space density of neutrinos cannot exceed the density of a degenerate Fermi gas. This puts an lower bound on the mass called the *Tremaine-Gunn* bound [48] which is a few hundreds of eV for dwarf galaxies and a few tens eV for galaxies [45]. Following these arguments, the SM neutrino cannot be a viable DM candidate.

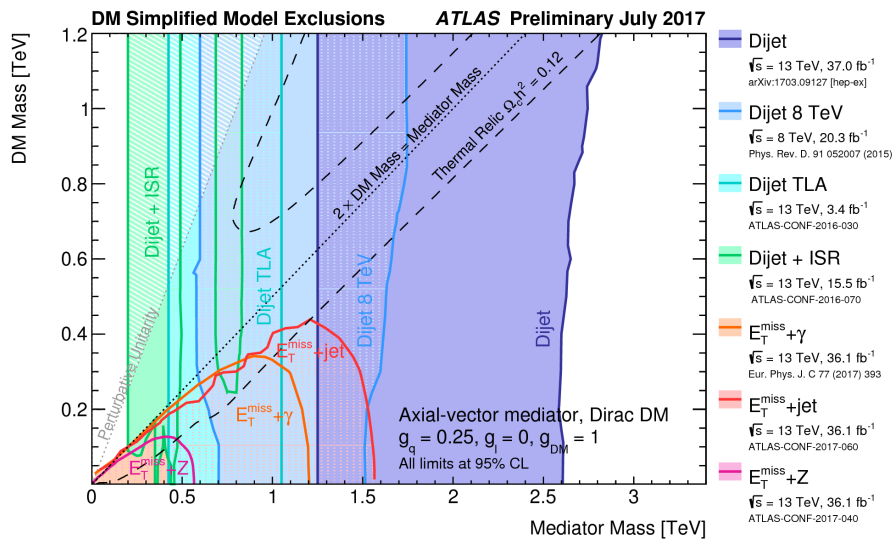


Figure 6: Limits on DM mass for the mass of a mediator using ATLAS data. Taken from [42].

A straightforward extension of the electroweak part of the Standard Model (SM) is the addition of right-handed neutrinos, or sterile neutrinos [49]. They are the hypothetical RH chiral counterparts of the LH neutrinos of the SM. Adding sterile neutrinos to the SM results in massive neutrinos therefore sterile neutrinos naturally explain neutrino flavour oscillations [45]. Since they are electrically neutral and right-handed, they are singlets under $SU(2) \otimes U(1)$: they do not take part in weak or electromagnetic interactions. They only interact with matter through mixing with active neutrinos. Sterile neutrinos not only naturally explain neutrino oscillations, they could also provide an explanation for the observed baryon asymmetry in the Universe [50]. They are therefore a very popular extension of the SM. To explain the two observed mass splittings (Δm_{sol}^2 , Δm_{atm}^2) in neutrinos in the SM, at least two additional sterile neutrinos are needed. But to also account for the observed DM today, it was shown that the minimal number of sterile neutrinos is 3 [50]. This model is called the *Neutrino Minimal Standard Model* (ν MSM) model. ν MSM solves three major problems for beyond the SM models [45]:

- Neutrino flavour oscillations
 - The absence of primordial antimatter
 - Dark matter

3.1.2 Production in the early Universe

Sterile neutrinos are neutral, long-lived and potentially massive particles and would therefore make an excellent DM candidate. But to be a viable DM candidate, sterile neutrinos also need to be produced efficiently in the early Universe.

A logical thought would be that a relic sterile neutrino density would also be produced in freeze out in the early Universe. Since sterile neutrinos are fermions as well, the Tremaine-Gunn bound on the mass of the sterile neutrino is the same as

for ordinary neutrinos: 0.4 keV [51]. Sterile neutrinos also have the same number density in equilibrium as ordinary neutrinos (112 cm^{-3}). Using these numbers the energy density today would be $\rho_{\text{sterile, eq}} \simeq 45 \text{ keV/cm}^3$ [51]. This is considerably larger than the critical energy density of the Universe. Sterile neutrino DM can therefore not be produced in a thermal freeze out.

Sterile neutrinos only interact with SM neutrinos via mixing, but this mixing is strongly suppressed at temperatures above a few hundred MeV [49]. Therefore DM sterile neutrinos are never in thermal equilibrium with the cosmological plasma and their number density is significantly smaller than that of active neutrinos. This is also the reason that they can account for DM without violating the Tremaine-Gunn bound. Sterile neutrinos are an example of decaying DM. Through its mixing with the ordinary neutrinos, a sterile neutrino can decay via Z boson exchange into three (anti)neutrinos [52], as shown if figure 7a.

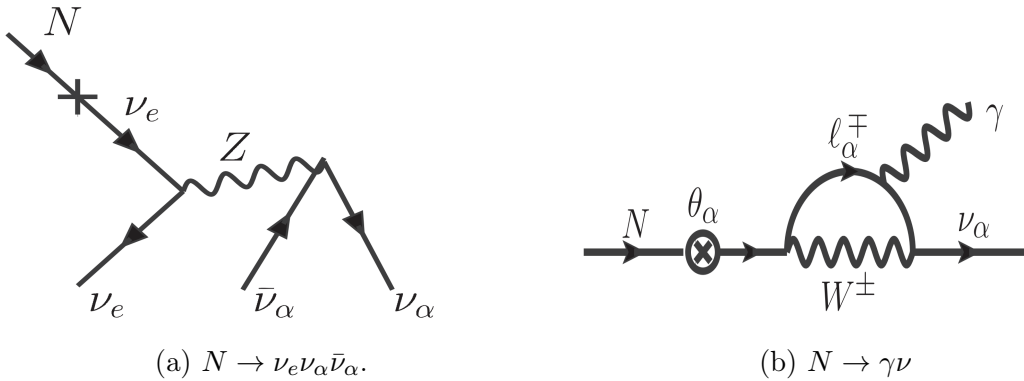


Figure 7: Left: Decay of sterile neutrino $N \rightarrow \nu_e \nu_\alpha \bar{\nu}_\alpha$ through neutral current interactions. A virtual ν_e is created and the quadratic mixing angle (marked by the symbol “ \times ”) is proportional to θ^2 . Right: Two-body decay of sterile neutrino. The energy of the photon is $E_\gamma = \frac{1}{2}M_N$. Figures taken from [45].

The total decay width for $N \rightarrow 3\nu$ is given by [51]:

$$\Gamma_{N \rightarrow 3\nu} = \frac{G_F^2 m_N^5}{96\pi^3} \sin^2 \theta = \frac{1}{4.7 \times 10^{10} \text{ sec}} \left(\frac{m_N}{50 \text{ keV}} \right)^5 \sin^2 \theta, \quad (18)$$

where G_F is the Fermi constant, m_N is the mass of the sterile neutrino and θ is the mixing angle. To be DM, the lifetime of the sterile neutrino should be larger than the lifetime of the Universe. This puts constraints on the mixing angle θ :

$$\theta^2 \lesssim 1.1 \times 10^{-7} \left(\frac{50 \text{ keV}}{m_N} \right)^5 \simeq 34.4 \left(\frac{\text{keV}}{m_N} \right)^5 \quad (19)$$

Besides the decay via a Z boson, sterile neutrinos can also decay into an active neutrino and a photon, see figure 7b. The total decay width for $N \rightarrow \gamma\nu$ is given by [52]:

$$\Gamma_{N \rightarrow \gamma\nu} = \frac{9\alpha G_F^2 m_N^5}{1024\pi^4} \sin^2 2\theta = 5.5 \times 10^{-22} \theta^2 \left(\frac{m_N}{\text{keV}} \right)^5 \text{s}^{-1}, \quad (20)$$

where α is the fine-structure constant. This puts a significantly stronger constraint on the mixing angle:

$$\theta^2 \lesssim 1.5 \times 10^{-5} \left(\frac{\text{keV}}{m_N} \right)^5 \quad (21)$$

From Eq. 19 and 21 follows that if θ is sufficiently small, sterile neutrinos are produced non-thermally. In the ν MSM dark matter sterile neutrinos are produced in the early Universe via mixing with active neutrinos. The fraction of energy of the present Universe from the sterile neutrino energy is [50]

$$\Omega_N h^2 \sim 0.1 \sum_i \sum_{\alpha=e,\mu,\tau} \left(\frac{|\theta_{\alpha i}|}{10^{-8}} \right) \left(\frac{m_i}{1 \text{ keV}} \right), \quad (22)$$

where \sum_i is the summation over the sterile neutrino N_i . As the production mechanism of sterile neutrinos is the oscillations between active and sterile neutrinos, there exists a resonance, analogous to the Mikheyev-Smirnov-Wolfenstein resonance for neutrino flavour oscillations [53]. For non-resonant production (NRP), the active-sterile neutrino mixing has a peak at [45]

$$T_{\text{peak}} = 130 \left(\frac{m_i}{1 \text{ keV}} \right)^{1/3} \text{ MeV}, \quad (23)$$

resulting in “warm” DM particles. Resonant production (RP) of sterile neutrino DM occurs in the presence of lepton asymmetry and results in much colder DM. To account for the observed DM the lepton asymmetry is about $\eta \sim 10^{-6} \left(\frac{\text{keV}}{m_N} \right)$, which is much larger than the observed baryon asymmetry ($\sim 10^{-10}$) [45]. RP sterile neutrino DM is fully compatible with astrophysical and cosmological observations, but also “warm” enough to suppress substructures in Milky-Way-size galaxies [51].

3.1.3 Searches for DM sterile neutrinos

Figure 8 shows the constraints on the parameter space for DM sterile neutrinos in the ν MSM model from cosmological experiments. The phase-space density constraints are related to the Tremaine-Gunn bound for sterile neutrinos, as discussed above. The X-ray constraints are due to the fact that sterile neutrinos can decay into photons ($N \rightarrow \gamma\nu$). Their decays therefore produce a narrow line in spectra of DM-dominated astrophysical objects. Many experiments such as XMM-Newton, Chandra, INTEGRAL and Suzaku aimed to discover these lines. None revealed any candidate lines in the ~ 0.5 keV -10 MeV energy range [52]. The Lyman- α bounds come from power-spectrum constraints from the CMB (for a review on the Lyman- α bounds, see [54]).

Besides astrophysical and cosmological searches, accelerator experiments also aim to find sterile neutrinos. If the masses of sterile neutrinos responsible for neutrino oscillations are below the electroweak scale, as in the ν MSM, they could in principle be found accelerator experiments [45]. These experiments use two strategies. The first is to detect the appearance of the decay products of sterile neutrinos. Properties of such decays can be found in [55]. The second strategy is to investigate the kinematics of rare meson decays [56].

Current data from astrophysical, cosmological and accelerator searches can be described by sterile neutrino DM. Future cosmological research will hopefully detect the imprints that sterile neutrino DM leaves in power spectra, while accelerator experiments hopefully find hints for sterile neutrino decays.

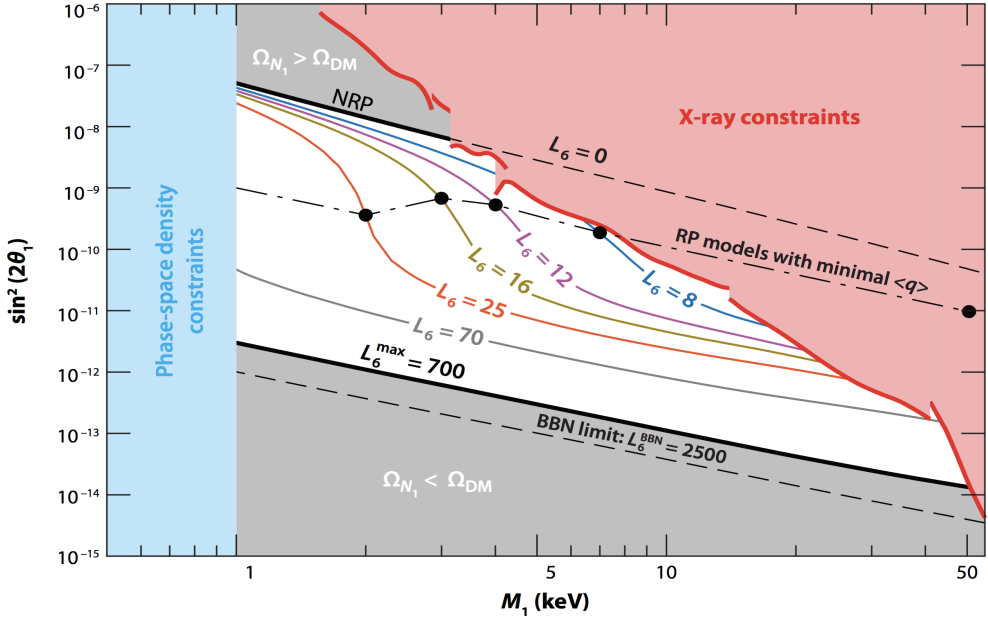


Figure 8: The allowed region of parameters for dark matter sterile neutrinos produced via mixing with active neutrinos (*unshaded region*). The two thick black lines bounding this region represent production curves for non-resonant production (NRP) and resonant production (RP). The red shaded region in the upper right corner represents X-ray constraints. The thin colored curves between thick black lines represent the production curves for different values of lepton asymmetry. The black filled circles are compatible with Lyman- α bounds and the X-ray bounds. The region below 1 keV is ruled out according to phase-space density arguments. Figure taken from [52].

3.2 Axions (Samuel)

In this section the axion, a hypothetical particle, will be discussed. It was introduced by Roberto Peccei and Helen Quinn in 1977 [57] as a solution to the strong CP problem. Later it was regarded as a possible dark matter candidate, due to its collisionless and non-relativistic behavior [58]. Some axion experiments are currently running, yet the searches have not resulted into finding these almost *invisible* particles.

3.2.1 Strong CP problem

The strong CP problem originates from the QCD gauge symmetry due to its non-Abelian nature [58]. In QCD, the gauge invariant vacuum state can be written as

$$|\theta\rangle = \sum_n e^{in\theta} |n\rangle \quad (24)$$

where θ is a parameter that describes the vacuum state $|\theta\rangle$. This θ can be interpreted as an angle, yet it is not invariant under transformation $\theta \rightarrow \theta - \sum_{i=1}^N \alpha_i$ and hence not observable [58]. However, $\bar{\theta} \equiv \theta - \arg \det \mathcal{M}$, with \mathcal{M} the quark mass matrix, is invariant and thus an observable.

The discrete symmetries imposed by the charge and parity operations are violated by the vacuum angle θ in QCD. In opposite to the expectation, CP violation is not observed in QCD. If there is CP violation present in QCD, the most simple observed consequence is an electric dipole moment for the neutron. This can be expressed as $|d_n| \approx 10^{-16}\bar{\theta}e$ cm, with e the electric charge. Currently, the limit on the dipole moment is determined experimentally at $|d_n| < 3.0 \times 10^{-26}e$ cm [59], implying $|\bar{\theta}| < 10^{-9}$. It is not expected for θ to be this small. Moreover, CP violation occurs due to complex quark masses and therefore, it is expected to have θ to be of the order 1 [58]. This discrepancy is called the strong CP problem. The question remains why θ is very small, while CP violation is present in the Standard Model.

3.2.2 The Peccei-Quinn solution

In 1977, Peccei and Quinn provided a solution to the strong CP problem. The parameter $\bar{\theta}$ is not interpreted as a parameter, yet plays the role of a dynamical variable [58]. The potential for this variable has a minimum and the variable naturally relaxes to the minimum of this potential. Hence, the value for θ is small. In order to incorporate the PQ solution, a spontaneously breaking global symmetry, $U(1)_{PQ}$ is necessary [60]. This symmetry replaces the CP violating angle $\bar{\theta}$ by a dynamical charge-parity conserving field. The implementation of this symmetry results in the existence of a Nambu-Goldstone boson, the axion, and $\bar{\theta}$ can be absorbed into its field a [58]. Moreover, non-perturbative effects make QCD depend on $\bar{\theta}$, which provides a potential for the axion, through which the axion obtains mass. The axion slides down to the potential's CP conserving minimum, the solution to the strong CP problem.

If axions exist, their couplings are extremely weak, their mass is extremely low and the lifetime could be very long [58]. Therefore, axions are sometimes called *invisible* and two important invisible axion models exist. In these models, the PQ symmetry decouples from the electroweak scale and spontaneously breaks at very high temperatures, which decreases the axion's mass and coupling strength. In the Kim-Shifman-Vainshtein-Zakharov (KSVZ) model, the axion is interpreted as the phase of an additional electroweak singlet scalar field. It couples to an additional heavy quark, an electroweak singlet as well. The Dine-Fischler-Srednicki-Zhitnitsky (DFSZ) model contains an additional electroweakly interacting scalar singlet. This singlet gains a vacuum expectation value when the PQ symmetry is broken [58]. These two models are dominant for axion research as they predict a band for the coupling strength and axion mass.

3.2.3 Axions as dark matter candidates

Besides the possible solutions to the strong CP problem, axions are a proper dark matter candidate for the following reasons:

1. Axions are non-relativistic (cold)
2. The population of axions could be present in sufficient quantities to provide the required energy density for dark matter
3. Axions are almost collisionless, the only long-range interaction is gravity

Cold axions are produced from equilibrium. The axions, if they are considered as dark matter candidates, are produced non-thermally due to the initial misalignment mechanism (see [61]). Actually, there are three different mechanisms through which cold axions are produced: vacuum realignment, string decay and domain wall decay. The mechanism that contributes the most to the axion population depends on the inflationary reheating temperature T_R . The axion production incorporates some notions of string theory and topology, which are beyond the scope of this review. For details on axion production through the three mechanisms see for example [62]. Here, only a qualitative overview of axion production is given.

Two important scales are present in axion dark matter production [58]. The first is the PQ symmetry breaking temperature T_{PQ} . The second scale is the temperature at which the axion mass, originating from non-perturbative QCD effects, becomes significant. At high temperatures, QCD effects are insignificant and the axion mass can be neglected [63]. The mass becomes important at critical time t_1 , when $m_a t_1 \sim 1$ and the temperature $T_1 \approx 1 \text{ GeV}$.

At early times and high temperatures (above T_{PQ}) the PQ symmetry is conserved. When the temperature equals T_{PQ} , the symmetry breaks and axion strings appear as topological defects. If T_{PQ} is higher than the inflationary reheating temperature T_R , the axion field is homogenized over large distances and the string density is diluted due to inflation. In opposite, if $T_{\text{PQ}} < T_R$, the axion field is not homogenized through the universe and strings radiate cold axions with zero mass. This process continues until T_1 is reached, when non-perturbative QCD effects become important. When T_1 is reached, the axion strings become boundaries of so called N domain walls. A domain wall is a type of topological defect that occurs in case of symmetry breaking. These walls radiate cold axions rapidly and eventually decay in case $N = 1$, implying $T_{\text{PQ}} > T_R$. If $T_{\text{PQ}} < T_R$, string and wall decay contribute to the axion energy density. If $T_R < T_{\text{PQ}}$ and, in addition, the axion string density is diluted due to inflation, only vacuum realignment will contribute significantly to the axion population [58].

Vacuum realignment produces cold axions, independent of the inflationary reheating temperature. At T_{PQ} , the amplitude of the axion field can have any arbitrary value. If $T_{\text{PQ}} > T_R$, inflation causes homogenization of the axions and the axion field will have a single value for the whole universe. The axion field has a potential due to non-perturbative QCD effects that cause the axions to oscillate. The oscillations do not decay due to very small couplings of the axion. Therefore the oscillations contribute significantly to the energy density of non-relativistic dark matter. Thus, cold axions originate from vacuum realignment, independent of the reheating temperature.

3.2.4 Experimental searches for axions

Axions are pseudoscalars and therefore can be produced in photon-photon interactions $\gamma\gamma^* \rightarrow a$, known as the Primakoff effect [64], which is shown in Figure 9. Photons interact electromagnetically, thus this process implies mixing between photons and axions in an electromagnetic field. In 1983, Pierre Sikivie thought of two ways to detect axions based on the Primakoff effect [65, 66].

The first method Sikivie pointed out is detection of axions originating from the sun's nuclear burning core [65, 66]. The Primakoff process is the mechanism through which the axions can be detected, $\gamma + Ze \rightarrow a + Ze$. The axions are detected by



Figure 9: Visualization of the Primakoff effect. Photons can convert into axions and vice versa in the presence of a very strong magnetic field [64].

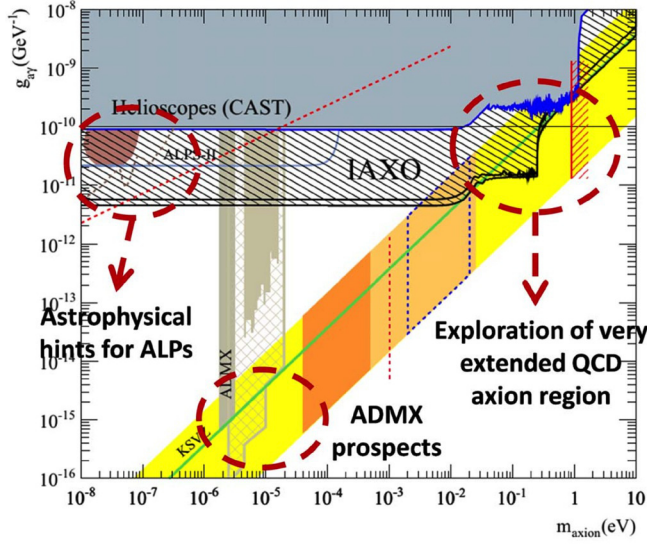


Figure 10: Mass and coupling strength regions for the axion. CAST and ADMX just probed the interesting band defined by the KSVZ and the DFSZ axion models. Clearly IAXO probes the interesting band considerably [68]

means of a helioscope. At CERN, one of the first axion helioscopes was built, called the CERN Axion Solar Telescope (CAST). With this helioscope the Peccei-Quinn model band could just be probed from which axions masses above 0.02 eV are excluded [67]. See Figure 10 for the CAST probing region.

The second method consists of a microwave cavity in a very strong magnetic field, where axions are converted into radio frequency photons. The cavity is tuned such that it meets the resonance condition $h\nu \approx m_a c^2$. Currently, the most sensitive microwave cavity experiment is the Axion Dark Matter eXperiment (ADMX). It has excluded a mass range between 1.9 and 3.5 μ eV for axions [69], see Figure 11.

The most promising axion detection experiment that is currently in development is the International AXion Observatory (IAXO). The method of measurement is similar to that of ADMX. This detector will be able to probe realistic and unexplored QCD ranges for the axion mass at the meV scale and above [71]. CAST's sensitivity is exceeded by a factor 10 approximately by IAXO. The main focus will be axions coming from cooling of white dwarfs.

3.3 Fuzzy Dark Matter (Rose)

Another theory for the origin of DM is what is known as Fuzzy Dark Matter (FDM). It is constituted of ultralight scalars, and the theory is posed as an alternative to

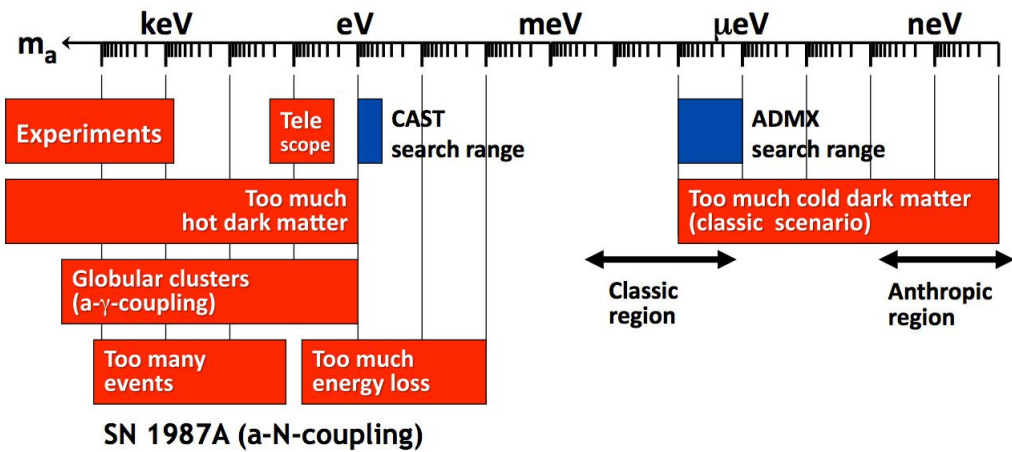


Figure 11: Excluded mass ranges (red) and regions of interest (blue) for the axion mass. The mass region of the scale of meV is not probed yet [70].

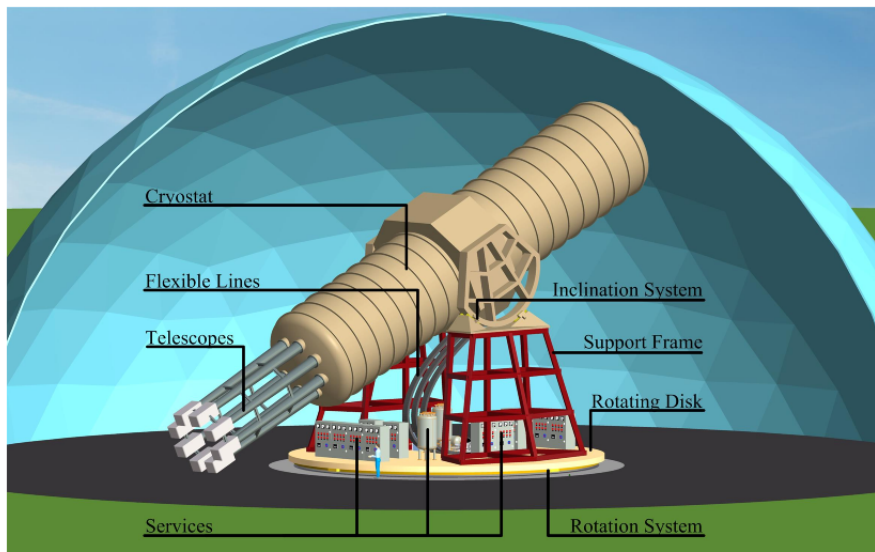


Figure 12: Schematic illustration of the IAXO. Multiple telescopes will possibly detect axions that are converted into photons due to the strong magnetic field that is present [71].

CDM. It has a mass $m \sim 10^{-22}$ eV and a de Broglie wavelength $\lambda \sim 1$ kpc [72]. While CDM is a well accepted theory for DM, there are several problems with it. Although it predicts large scale effects that are consistent with our observations, the theory cannot account for small scale structures. On galactic scales, although it has not been strictly modeled, naïve predictions yield results that are entirely inconsistent with our observations. They predict core densities larger than observed and a cusp with density $\rho \sim r^{-1}$, which are not observed [73]. The density of dwarf galaxies have a density much lower than predicted from CDM. Obviously, the physics on these scales is very complicated, and the referenced paper allows an explanation in the form of 'baryonic physics'. There is a theory in between CDM and HDM, known as Warm Dark Matter (WDM). The thermal velocity distribution has significant, nonlinear, gravitational effects on structure formation [74]. The large de Broglie wavelength allows the FDM to suppress small scale structures while still giving same predictions as CDM for large scale structures.

3.3.1 Light Spin Zero Fields

When the mass and the spin of a particle are exactly zero, there is an additional shift symmetry in the action.

$$S = \frac{1}{2} \int d^4x \sqrt{-g} g^{\mu\nu} \partial_\mu \phi \partial_\nu \phi \quad (25)$$

This symmetry is given by $\phi \rightarrow \phi + c$, where c is any constant. However, this symmetry is broken by the introduction of many other terms, for example a mass term in the form $m^2\phi^2$, a potential term, $V(\phi)$ or interaction terms with other fields. While the mass of the scalar must be non-zero to account for the gravitational effects seen by DM particles, we can impose the mass to be very light, giving us an approximate shift symmetry, which we expect to be broken on some level.

However, we could also consider an angular field, taking an action in the form,

$$S = \int d^4x \sqrt{-g} \left(\frac{F^2}{2} (g^{\mu\nu} \partial_\mu a \partial_\nu a) - \mu^4 (1 - \cos a) \right) \quad (26)$$

It is clear to see there is a shift symmetry for $c = 2\pi$. As a is dimensionless, the variable F has been introduced via dimensional analysis. The shift symmetry does allow us to add any higher harmonics, but the value of μ that is required to account for DM effects will cause the coefficients of the higher harmonics to be negligible [72]. These particles can arise naturally from other theories, i.e we see them in theories that weren't designed to predict them. All theories of particle physics derived from string theory contain at least a few of these particles ([75], [76], [77]). For this particle, the mass takes the form

$$m = \frac{\mu^2}{F} \quad (27)$$

and it is required to be $\sim 10^{-22}$. There have been bounds placed on F . The lower bound is approximately 10^{16} , the model independent axion of the weakly coupled heterotic string [78]. The upper bound is given by the Planck mass, giving us

$$10^{16}\text{GeV} \lesssim F \lesssim 10^{18}\text{GeV} \quad (28)$$

The expression for μ is generated by nonperturbative effects from the instanton. A good approximation is [72]

$$\mu^4 \sim M_{pl}^2 \Lambda^2 e^{-S} \quad (29)$$

where S is the action for the instanton and Λ is a suppression of instanton effects due to supersymmetry. These range from

$$10^4 \text{GeV} \lesssim \Lambda \lesssim 10^{18} \text{GeV} \quad (30)$$

which is a range of maximal to no suppression. This also gives bounds on S [79], although this is model-dependent. S can also vary with the volume of the cycle, leading to exponential changes in the mass [80].

The equation of motion for these particles is

$$D_\mu D^\mu a + m^2 a - \frac{m^2}{6} a^3 + O(a^6) = 0 \quad (31)$$

now we will show if we can really neglect self-interaction compared to its gravitational effects as claimed. Given a body with ϵ , a dimensionless gravitational potential, we would need

$$m^2 a^3 \gtrsim \epsilon m^2 a \quad (32)$$

or, $a^2 \gtrsim \epsilon$. At the temperature where the field begins to oscillate, T_0 , we have $a^2 \sim 1$ [72], $\epsilon \sim 10^{-5}$, the primordial cosmic fluctuations [81]. We see that indeed the condition is satisfied. Since $a \sim R^{-3/2}$, where R is the scale factor of the universe, and $R \sim 1/T$, we see we require $T = 10^{-5/3} T_0$ for gravitational effects to dominate. Given a value $T_0 = 500$ eV, we know that the gravitational effects will dominate in time for the radiation-matter equality, $T_{\Omega_m=\Omega_r} \sim 1$ eV.

Looking at today's universe, we roughly have $\epsilon \sim G\rho L^2 \sim GF^2 m^2 a^2 L^2$, with an object of length L and density ρ . This leaves us with the condition

$$L \gtrsim \frac{\sqrt{G}}{Fm} \quad (33)$$

which is equivalent to saying gravitational effects dominate with sizes larger than 1 pc.

3.3.2 Astrophysical Consequences

To see systems where the self-interaction of the FDM dominates, we must look at smaller scales. This means we can look inside the Milky Way or nearby systems to see the effects of FDM. Also considering, in the CDM model, small scale structures form first, we can look at objects with a large redshift. Let us consider Jean's instability. This occurs when the gas pressure is not large enough to prevent gravitational collapse in interstellar gas clouds [82]. FDM is unstable for masses greater than the Jean's mass. The Jeans radius is given by [83],

$$R_J = \frac{2\pi}{k_J} = \left(\frac{\pi^3}{G\rho m^2} \right)^{1/4} = 55 \left(\frac{10^{-22} \text{eV}}{m} \right)^{1/2} \left(\frac{2.8 \times 10^{11} M_\odot \text{Mpc}^{-3}}{\rho} \right)^{1/4} \quad (34)$$

below this scale perturbations are stable and above it the system will behave as CDM. To give a feeling for the magnitude of the de Broglie wavelength, consider

$$\frac{\lambda}{2\text{kpc}} = \left(\frac{10^{-22} \text{eV}}{m} \right) \left(\frac{10 \text{km/s}}{v} \right) \quad (35)$$

If we consider v as the Virial velocity in the de Broglie wavelength, $\lambda = \hbar/mv$, we would return the Jeans radius. It follows from the uncertainty principle (up to factors of \hbar)

$$R_J \lambda^{-1} \sim 1 \quad (36)$$

and we that R_J is a point of stability, increasing the momentum will allow the particles more spatial freedom². From this condition, we have an approximate bound on the maximum value for r for a self-gravitating system in equilibrium,

$$r \gtrsim \frac{\hbar^2}{GMm^2} \quad (37)$$

This is only an approximate statement but in general it holds. It also gives us a bound on the central density

$$\rho_c \lesssim \left(\frac{Gm^2}{\hbar^2} \right)^2 M^4 \quad (38)$$

The upper limit here is comparable to the observed central densities of dwarf galaxies [84]. Looking at the Jeans scale for a FDM halo gives

$$R_{JH} \sim 3.4 \left(\frac{c_{10}}{f_{10}} \right)^{1/3} \left(\frac{10^{-22} \text{eV}}{m} \right)^{2/3} M_{10}^{1/9} (\Omega_m h^2)^{-2/9} \text{kpc} \quad (39)$$

where $f_{10} = f(c)/10$, $f(c) = c^3/\ln(1+c) - \frac{c}{1+c}$, $c = c/10$ and $M_{10} = M/10^{10} M_\odot$. Making some assumptions, we can see for smaller halos there is no region with $\rho \sim r^{-1}$, and for larger halos the length of the cusps with r^{-1} dependence has been reduced from the Virial radius to R_{JH} [83]. As stated, the difference between the CDM model and FDM model arises when the de Broglie wavelength λ is comparable to the radius of our object.

If dark matter is FDM, the occupation numbers in galactic halos will be so high the dark matter will behave as a classical field obeying

$$\square\phi = m^2\phi \quad (40)$$

Using the Schrödinger-Poisson equation we would find

$$\nabla^2\epsilon = \frac{4\pi G}{a}\rho_0(|\phi|^2 - 1) \quad (41)$$

where $\rho_0 = \frac{3H_0^2}{8\pi G} = mn_0$, the mass density of the universe. Solving this equation in the region $0 < x < L$, with boundary conditions $\phi(0) = \phi(L) = 0$, along with an initial density variation at $t = 0$, $\delta\rho = \rho_0 \sin(\frac{\pi x}{L}) \gg \rho_b$, where $\rho_b = 2.8 \times 10^{11} \Omega_m h^2 M_\odot \text{Mpc}^{-3}$ is the background density is modeled in Figure 13 [83]. There is also a CDM simulation plotted with the same initial conditions.

With the condition $R_J \gg L$, there were no gravitational halos being formed. On the order $R_J \sim L$, we see a gravitational halo but no cusp. We also see a decrease in the core density. For $R_J \ll L$, we see the same effect as the CDM model.

²It is important at this point to note that λ has been tuned to take R_J to the scales of the structures we wish to remove. These are on the scale of the cores of dwarf galaxies, where we wish to suppress the core density. From this, it can be seen we have tight bounds on the mass of these particles, and it has been specifically chosen at $m = 10^{-22}$ to cause the effects we wish to observe.

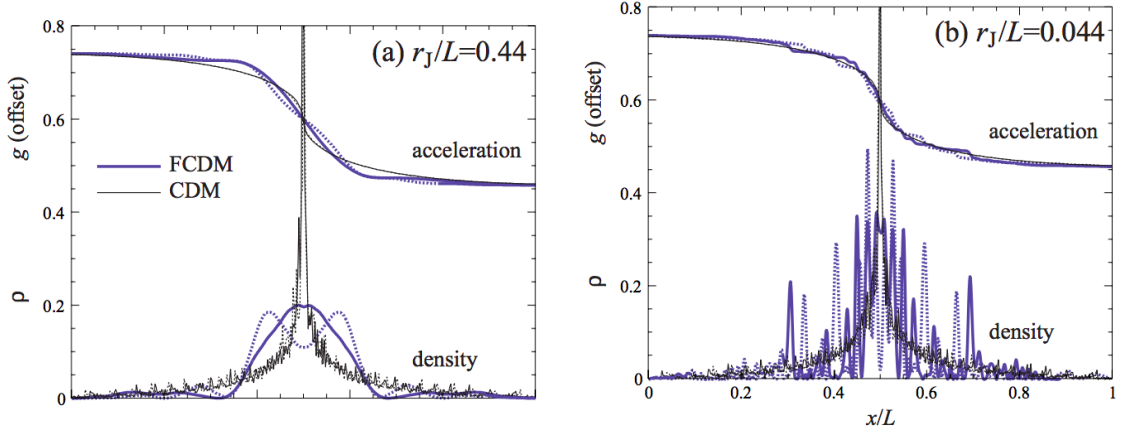


Figure 13: One dimensional simulations (a) large Jeans scale $R_J/L = 0.44$ (b) small Jeans scale $R_J/L = 0.044$. Two snapshots, $t/t_{dyn} = 99$ (solid) and 100 (dotted) are shown for the density profile (units of $15\rho_0$) and gravitational acceleration (units of $3L/2t_{dyn}^2$, offset for clarity). Figure taken from [83].

3.3.3 Final remarks

Although one may have concerns about this argument, having bosons with such a light mass may appear unphysical. However, due to the extra symmetry arising from a spinless ultralight scalar coupled to only gravity, it is a very natural argument. This particle would not have been detected from current experiments due to its ultra-light mass. It has been shown that the theory of FDM can suppress the cusps and reduce the core density in cusps. These effects appear to have a cut-off at $r \sim R_J$.

Due to a lack of literature on this topic, this review mostly follows [72] for the physical motivation and [83] for astrophysical consequences. Special thanks to these authors.

3.4 WIMPzillas (Davey)

In most theories of dark matter, dark matter particles are assumed to be thermal relics, particles that were once in local thermal equilibrium in the hot plasma that existed shortly after the Big Bang, until the rate at which they annihilated became lower than the rate at which the Universe expanded, leading to the so called dark matter freeze out, after which they were too far apart to annihilate. The reason this theory is so wildly popular is that this puts the expected annihilation cross section of a DM particle nicely on the scale of the weak interaction. However, this puts a limit on the mass of a dark matter candidate through the so-called unitarity bound. As the annihilation cross section scales inversely with the squared mass, this means heavier thermal relics would be more abundant in our universe, and thus the relic density we observe today puts an upper bound on the mass to avoid overclosing the universe. This limit is about $m_{DM} < 300$ TeV[24].

So far, no experiments have been able to detect WIMPs or other thermal relics in this expected mass range, opening the door for theories regarding more massive particles. One of these is the WIMPzilla, a superheavy particle with a mass above 10^{10} GeV. In this section the general properties, production mechanisms as well as

one of the major motivations for WIMPzillas will be discussed, starting with the general properties.

3.4.1 WIMPzilla properties

As stated before, the unitarity bound puts a limit on the allowed mass of a thermal relic. Therefore, if dark matter consists of WIMPzillas, which are far above that mass limit, they could not have been in thermal equilibrium at the time they decoupled from the hot plasma and are thus *nonthermal* relics. Instead of being produced in freeze-out, they are theorized to be produced in the inflationary epoch, something that will be treated in a bit more detail in the next section.

Secondly, WIMPzillas are expected to be very massive, with $m > 10^{10}$ GeV. This could put the WIMPzilla on the inflation mass scale of $m \approx 10^{12}$ GeV or on the GUT scale of $m \approx 10^{16}$ GeV, at which the WIMPzilla is also called the GUTzilla.[85]

Another important criterium for a WIMPzilla is that it needs to be stable or at least have a very long lifetime. As we still observe the effects of dark matter today, the particle that causes these effects needs to be stable enough to have lived to this day. One of the major arguments for WIMPzillas when they were first theorized was that their decay or annihilation could explain the observation of cosmic rays above the GZK-cutoff. This will be explained in further detail later, in section 3.4.3.

Lastly, WIMPzillas are expected to be cold dark matter, as mechanisms to accelerate these superheavy particles to relativistic velocities are unknown as of yet.

3.4.2 WIMPzilla production

While the production mechanism for thermal relics is well understood and dark matter particles arise nicely from it, the production mechanism for nonthermal relics is mostly unknown at the moment. Due to the energy scales needed to produce these superheavy particles, most theories assume their production to happen shortly after the inflationary epoch of the Universe or during the time when the temperature of the universe was at or above the GUT scale. As these theories are numerous and can be quite complex, they are beyond the scope of this review. Thus, only the qualitative description of some of these theories will be given with references to articles that cover them and other theories in more detail.

First off, there is production of WIMPzillas during reheating. At the end of inflation, the Universe was in a cold state, as the particles that were around before inflation were now spread out over a very large volume. As the Universe now is again in a hot and dense state, something has had to have happened to produce a large amount of energy and particles. This process is generally believed to be reheating. During reheating, the inflaton field decayed and its potential energy, which was very large, was converted into energy which produced particles much more massive than the reheating temperature of 10^{10} GeV. One of these particles could then be the WIMPzilla.[86] For a more in depth discussion of WIMPzilla production during reheating, see [85][86][87].

Secondly, there is gravitational production of WIMPzillas. In this process, which takes place in the era between inflation and matter/radiation-domination, WIMPzillas are produced as a result of the expansion of the background spacetime acting on the vacuum fluctuations of the WIMPzilla field. To fulfill the relic density we observe today, the WIMPzilla mass would need to be on the order of the inflaton mass if

they were produced in this process. What makes this interesting is that somewhere in the future, the inflaton mass could be calculated, which would also determine the mass scale of the WIMPzilla. To read more about gravitational production, see [88].

As the WIMPzilla is only a hypothetical particle, many other theories for the production of WIMPzillas have been published. For a small selection of these, refer to [89][90][91][92][93].

3.4.3 The GZK-limit and WIMPzillas

When the WIMPzilla was first introduced, one of its main motivations was that its decay or annihilation could explain the observation of ultra-high energy cosmic rays above the so-called Greisen–Zatsepin–Kuzmin(GZK) limit. As it was widely believed that these ultra-high energy cosmic rays consisted mainly of intergalactic protons, it was theorized that above an energy of 5×10^{19} GeV they would interact with CMB photons and produce Δ^+ resonances which then would decay into neutrons/protons and pions following

$$\begin{aligned}\gamma_{CMB} + p &\rightarrow \Delta^+ \rightarrow n + \pi^+, \\ \gamma_{CMB} + p &\rightarrow \Delta^+ \rightarrow p + \pi^0,\end{aligned}$$

which would strongly suppress the cosmic ray flux above these energies. This flux suppression is the GZK-limit. Cosmic rays above this limit could then possibly be produced in the decay or annihilation of superheavy particles like the WIMPzilla. While this flux suppression has been observed, recent results by for instance the Pierre Auger Telescope have shown that the composition of ultra-high energy cosmic rays is not purely protonic, but instead is a mix of nuclei and protons, with the mix being heavier at higher energies.[94] While this result makes this specific argument for WIMPzillas obsolete, it does not mean that WIMPzillas can be ruled out completely, although detecting them will be a difficult task.

4 Primordial Black Holes

4.1 Motivation for Primordial Black Holes (Rose)

Due to the extreme conditions of the early universe, they can be considered a breeding ground for Primordial Black Holes (PBHs). PBHs are formed before Big Bang Nucleosynthesis (BBN) and are therefore non-baryonic. Specifically, they are formed when the Schwarzschild radius is comparable to the Hubble radius [95]. Dynamically, they behave as cold objects and are therefore viable candidates for DM. PBHs are also predicted from string theory considering an extra compactified dimension in the braneworld theory [96].

Most candidates for DM require a theory which predicts a new particle, while it is nice to see naturally occurring DM candidates in other theories, each theory often has its own set of problems and free parameters [27]. A bonus of PBHs are they require no extension to the SM, and they occur naturally in the well-established theory of inflation. They will grow by accreting matter they attract gravitationally.

We can put a number of constraints on the possible masses of these stellar objects. Due to Hawking radiation, they must have a mass which allows the evaporation time to be larger than the Hubble time [97]. The evaporation time is given by $t_{\text{ev}} \approx 10^{10} (M_{\text{PBH}}/10^{15} \text{g}) \text{yr}$. Therefore our first constraint takes the form $M_{\text{PBH}} > 10^{-15} \sim 10^{-18} M_{\odot}$, as any PBH with a lower mass will have evaporated [98]. Fortunately, in this range PBHs will indeed behave as dynamically cold objects.

There have been many experimental constraints put onto the masses of these objects. They are summarised in Figure 14.

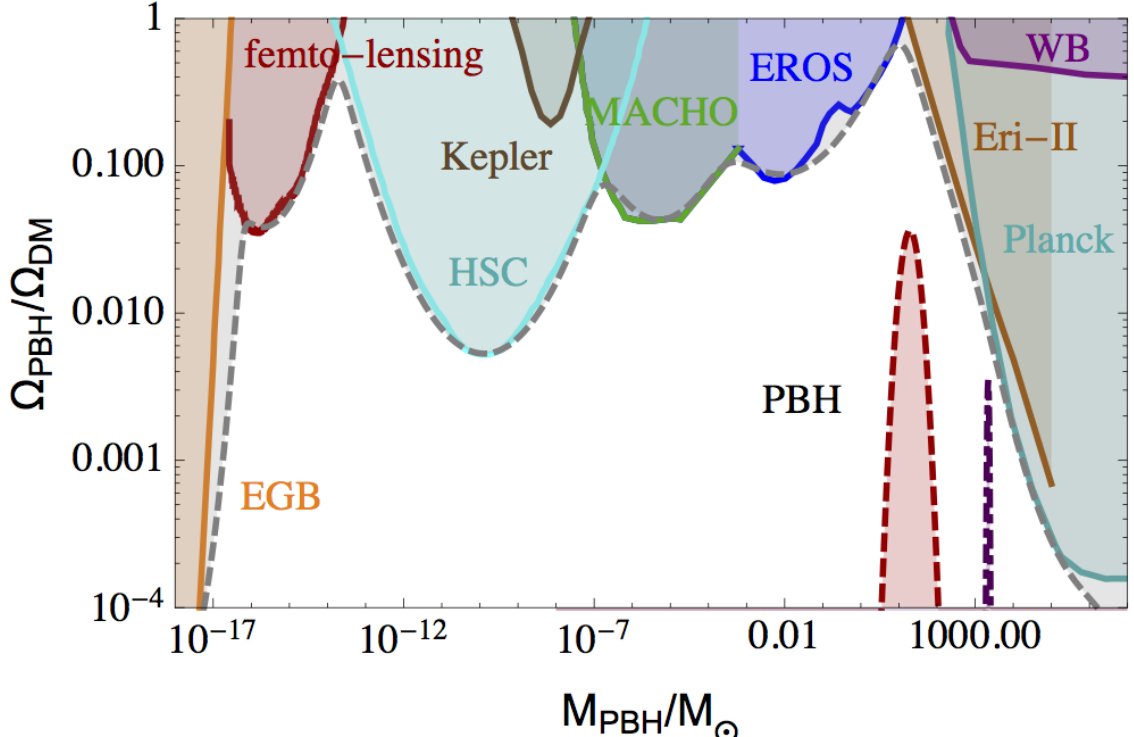


Figure 14: Observational constraints on PBH from a plethora of experiments (for a review see [99]). Clearly the final PBH distribution passes all constraints, and at the same time constitute all of dark matter. Figure taken from [100].

4.2 PBH Capture (Rose)

Looking at the astrophysical effects of PBHs, a constraint can be made for the number of PBHs in a halo. PBHs will not accrete the interstellar medium (ISM), although they can be gravitationally captured by stars while they are being formed in a Giant Molecular Cloud (GMC).

First we need to find the distribution of PBHs in the Milky Way. From the Cored Spherical Isothermic (CSI) model, we can approximate the density of the dark matter halo as [101]

$$\rho(r) = \frac{a^2}{a^2 + r^2} \quad (42)$$

where a is the core radius. This leads us to the density distribution of CDM in the Milky Way.

$$\rho_{\text{CDM}}(R, z) = \rho_{\text{CDM}}(R_0, 0) \left(\frac{a^2 + R_0^2}{a^2 + R^2 + z^2} \right) \quad (43)$$

Here we are using Galactocentric coordinates, R_0 is the distance to the Galactic centre. We can expect the overdensity of PBHs to be comparable to that of CDM, giving us

$$n_{\text{PBH}}(R, z) M_{\text{PBH}} \approx \rho_{\text{CDM}}(R, z) \left(\frac{\Omega_{\text{PBH}}}{\Omega_{\text{CDM}}} \right) \quad (44)$$

To show some typical values for this [102],

$$n_{\text{PBH}}(R, z) \approx 1.8 \cdot 10^{-39} \left(\frac{10^{15} \text{g}}{M_{\text{PBH}}} \right) \left(\frac{a^2 + R_0^2}{a^2 + R^2 + z^2} \right) \Omega_{\text{PBH}} \text{ cm}^{-3} \quad (45)$$

Comparing this to a Gaussian distribution with a one-dimensional velocity dispersion σ , we would find the 3-dimensional distribution of PBHs as

$$f_{\text{PBH}}(R, z, v) = \frac{n_{\text{PBH}}}{(2\pi\sigma)^{3/2}} e^{-\frac{v^2}{2\sigma^2}} \quad (46)$$

In order to find the number of PBHs that will be captured by stars as they form, we will consider the Universe in a time when the Milky Way was a GMC. These will have a typical diameter of 10–50 pc and mass $10^{37} - 10^{39}$ g [103]. Before any stars have formed, a typical distribution of unbound PBHs in this GMC is simply the product of the distribution found in Equation 46 with the volume of the GMC. This gives us

$$N_{\text{PBH},i}(R, 0) \approx 2.2 \cdot 10^{20} \left(\frac{10^{15} \text{g}}{M_{\text{PBH}}} \right) \left(\frac{a^2 + R_0^2}{a^2 + R^2} \right) \quad (47)$$

As a GMC begins to collapse, the PBHs will lose energy as they become gravitationally bound. Eventually they will lose enough energy to remain inside the star. This energy loss will then take the form

$$E_{\text{loss}} > \frac{M_{\text{PBH}} v_0^2}{2} \quad (48)$$

Where E_{loss} is the energy loss required to capture PBH and v_0 is the asymptotic velocity of the PBH. This energy loss occurs in two ways: dynamical friction and deceleration due to accretion. For PBHs greater than the evaporation mass, dynamical friction is the force that will dominate. Given $f_{\text{dyn}} = -4\pi G^2 M_{\text{PBH}}^2 \rho \ln \Lambda \mathbf{v} / v^3$ [104], we find energy loss in the form

$$E_{\text{loss}} = \frac{4G^2 M_{\text{PBH}}^2 M}{R^2} \left\langle \frac{\ln \Lambda}{v^2} \right\rangle \quad (49)$$

where M and ρ are the mass and density of the star, $\ln \Lambda$ is the Coulomb logarithm [105] and v is the PBH velocity. The $\langle \dots \rangle$ denote the density-weighted average. Following [106], we see the time scale for an object like this to collapse is given by

$$t_c = \frac{\phi_{\text{GMC}}}{\partial \phi_{\text{GMC}} / \partial t} \quad (50)$$

Where ϕ_{GMC} is the clouds gravitational potential. Using $-\phi_{\text{GMC}} \sim GM/R \sim v_f^2$, where v_f is the freefall velocity. This gives us

$$\frac{v_c}{v_f} \lesssim \left(\frac{t_f}{t_c} \right)^{1/3} \quad (51)$$

The most realistic situation is a slow contraction, i.e. $t_c \gg t_f$. We find that the average number of PBHs captured by each star will be

$$N_{\text{PBH},c} = 1.9 \cdot 10^{12} \delta \left(\frac{10^{15} \text{g}}{M_{\text{PBH}}} \right) \left(\frac{a^2 + R_0^2}{a^2 + R^2} \right) \quad (52)$$

where δ is some dilution factor to account for only about 40% of the mass of a GMC will be formed into stars. This means each forming star will capture 1 PBH if

$$M_{\text{PBH}} < 1.9 \cdot 10^{37} \delta \left(\frac{a^2 + R_0^2}{a^2 + R^2} \right) \Omega_{\text{PBH}} \quad (53)$$

When a PBH gets captured by a star, due to the dynamical friction, it will tend towards the barycenter if its mass is larger than its companion star. It will begin to accrete mass from the donor star. The mass of the PBH will increase with time, and the accretion will have a corresponding luminosity. This luminosity will increase until it is comparable with that of the original luminosity of the star. With enough time, the entire star will be swallowed by the PBH. The luminosity will increase until it reaches the Eddington luminosity.

We shall briefly turn our attention to the Bondi accretion theory, a good model for our situation. This has an accretion radius of [107]

$$R_{\text{acc}} \approx 1.5 \cdot 10^{-4} \left(\frac{M_{\text{PBH}}}{10^{15} \text{g}} \right)^2 \left(\frac{10^4}{T} \right) \quad (54)$$

Any object closer than the PBH than this radius will be accreted. We also have a corresponding equation for the rate of accretion

$$\frac{dM}{dt} \approx 9.5 \cdot 10^4 \left(\frac{M_{\text{PBH}}}{10^{15} \text{g}} \right) \left(\frac{\rho}{\text{g cm}^{-3}} \right) \left(\frac{10^4 \text{K}}{T} \right)^{3/2} \text{g yr}^{-1} \quad (55)$$

here ρ and T are the density and temperature of matter at R_{acc} . The accretion luminosity is given by

$$L_{\text{acc}} \approx \epsilon c^2 \frac{dM}{dt} \quad (56)$$

where ϵ is a measure of efficiency. The Eddington luminosity is given by [102]

$$L_E \approx 6.5 \cdot 10^{19} \left(\frac{M_{\text{PBH}}}{10^{15} \text{g}} \right) \text{erg s}^{-1} \quad (57)$$

When the accretion luminosity reaches the Eddington luminosity, the accretion will become Eddington limited. We recall the Eddington luminosity is the maximum luminosity a body can reach whilst the radiation pressure can still balance the gravitational force. Beyond this luminosity there are extreme stellar winds. The limited accretion rate is given by

$$\frac{dM}{dt} \approx 2.3 \cdot 10^6 \epsilon^{-1} \left(\frac{M_{\text{PBH}}}{10^{15} \text{g}} \right) \text{g yr}^{-1} \quad (58)$$

We now ask ourselves the fate of the star. Considering a star with comparable properties as our Sun, we would find the accretion luminosity would be given by

$$L_{\text{acc}} \approx 8.6 \cdot 10^{14} \epsilon \left(\frac{M_{\text{PBH}}}{10^{15} \text{g}} \right)^2 \text{erg s}^{-1} \quad (59)$$

From here we can see we would find 3 regimes [102]

Accretion always in Bondi regime

This gives us the condition $L_{acc}(t) < L_E(t)$, $\forall t$. We would find the condition $M_{\text{PBH}} < 7.6 \cdot 10^{24}$ g (using $\epsilon \approx 10^{-5}$), and therefore $M_{\text{PBH}} < M_*$. The presence of the PBH here is not detrimental to the star. This time is independent of M_* .

Accretion always Eddington limited

To satisfy this we must find $L_{acc}(0) > L_E(0)$, where t is some initial time. We would find the condition $M_{\text{PBH}} > 7.6 \cdot 10^{24}$ g, and therefore $M_{\text{PBH}} \sim M_*$. The star will have a period of time $t \sim 10^4$ yr where the star will be overluminous, and after which it will be entirely swallowed by the PBH.

Accretion begins in Bondi regime, becomes Eddington limited

For this to occur, we would have $L_{acc}(0) < L_E(0)$, then $L_{acc}(t_{to}) > L_E(t_{to})$ where t_{to} is some turnover time. In order to get the initial conditions, we find $M_{\text{PBH}} < 7.6 \cdot 10^{24}$ g, but eventually finding a turnover time gives us $M_{\text{PBH}} > 2.6 \cdot 10^{18}$ g. The turnover time is approximately $t_{to} \approx 1.3 \cdot 10^{10}$ yr. After this, the process will continue as described in **always Eddington limit**.

We see we have begun by assuming each forming star gravitationally captures a PBH. If $M_{\text{PBH}} > 10^{20}$ g, we see the PBH will swallow its companion star on a timescale much less than the Hubble time. In fact this will happen for any star with a mass greater than the evaporation mass. From this we can easily conclude that only a small number of stars will have gravitationally captured PBHs. Equation 53 must be violated. If we take $\delta \approx 0.1$, a reasonable value for the efficiency of star formation in a GMC. This tells us $M_{\text{PBH}} \gg 10^{25}$ g for any reasonable contribution to DM. This is about $M_{\text{PBH}} \gg 10^{-8} M_\odot$.

We can constrain these results even further following by considering capture of PBHs by neutron stars (NS) [104]. Looking again at Equation 49, we know $E_{loss} \sim 1/R$, and therefore NSs will capture PBHs most efficiently. They will be swallowed by any companion PBH. NSs also slow the PBHs faster via accretion. This gives us a modified energy loss

$$E_{loss}/M_{\text{PBH}} \approx 6.3 \cdot 10^{-12} \left(\frac{M_{\text{PBH}}}{10^{22} \text{g}} \right) \quad (60)$$

Through a short analysis (see [104] for more details), we find the time for this energy loss is given by

$$t_{loss} \approx 4.1 \cdot 10^4 \left(\frac{M_{\text{PBH}}}{10^{22} \text{g}} \right)^{-3/2} \text{yr} \quad (61)$$

So for a star to be captured on a time less than 10^{10} yr, we have $M_{\text{PBH}} \gtrsim 2.5 \cdot 10^{18}$ g. Once the PBH has been captured, it will swallow the NS fairly quickly. We can estimate the capture rate of NSs using the density of PBHs. We require that the capture rate is much less than 1, due to our current observations of NSs. This leads us to

$$\frac{\Omega_{\text{PBH}}}{\Omega_{\text{DM}}} \leq \frac{1}{t_{NS} F_0} \quad (62)$$

where F_0 is some initial capture rate, depending on the environment the NS is in. While this doesn't give us a strict bound on the masses, it does give us a restriction on how much DM is constituted of PBHs in particular mass regimes.

4.3 The merger rate of PBH binaries (Gabriël)

4.3.1 Did LIGO detect dark matter?

Chapline was the first to suggest primordial black holes (PBHs) as a dark matter candidate in 1975 [108]. Since then the idea of PBHs as DM candidate has been surpassed by the notion of DM being a new elementary particle. However, recently PBH dark matter regained attention when LIGO first detected the merging of two black holes [5]. This is because the estimated masses of the merger were $\sim 30M_\odot$. The range of theoretically possible masses of PBHs spans 90 orders of magnitude but most of it has been excluded by various null observations of expected signatures of their interaction with standard astrophysical objects [109]. However, in the window for masses $20M_\odot \lesssim M_{\text{PBH}} \lesssim 100M_\odot$ these constraints are a lot less robust. Since the estimated masses of the black holes in the merger are within this window, Bird et al [110] suggested the possibility that LIGO detected PBH dark matter. A way to probe this is to examine the merger rate. If PBHs in a certain mass window account for all or a fraction of the DM in the Universe, an excess of merger events should be seen involving black holes with corresponding masses [111]. If this excess is significantly larger than the expected background of mergers of traditional astrophysical black holes, gravitational wave detectors could in principle detect PBHs or put limits on their abundance.

4.3.2 The close encounter scenario

The goal is to determine whether or not the merger rate of PBHs with masses $\sim 30M_\odot$ falls within the merger rate that can be inferred from gravitational wave detections. If this turns out to be the case, there is a possibility that DM consists of these PBHs. A model of PBH binary formation was proposed in Ref. [110]. In this model two PBHs in the present day Universe approach each other with a relative velocity v_{pbh} , producing a time-varying quadrupole moment and thus GW emission. They form a binary if the GW emission exceeds the initial kinetic energy. The cross-section for this process is

$$\begin{aligned} \sigma &= \pi \left(\frac{85\pi}{3} \right)^{2/7} R_s^2 \left(\frac{v_{\text{pbh}}}{c} \right)^{-18/7} \\ &= 1.37 \times 10^{-14} M_{30}^2 v_{\text{pbh}-200}^{-18/7} \text{pc}^2, \end{aligned} \quad (63)$$

where M_{30} is the PBH mass in units of $30M_\odot$, $R_s = 2GM_{\text{pbh}}/c^2$ is its Schwarzschild radius and $v_{\text{pbh}-200}$ is the relative velocity of the two PBHs in units of 200 km sec^{-1} [110]. Assuming that all DM in the Universe resides in Milky-Way like halos, it is possible to calculate the rate of mergers per halo:

$$\begin{aligned} N &\simeq \frac{1}{2} V (\rho/M_{\text{pbh}})^2 \sigma v \\ &\simeq 3.10 \times 10^{-12} M_{12} \rho_{0.002} v_{\text{pbh}-200}^{-11/7} \text{yr}^{-1}, \end{aligned} \quad (64)$$

where V and ρ are the volume and density of the halo, assuming $M = M_{12}10^{12}M_\odot$ and $\rho = 0.002\rho_{0.002}M_\odot \text{ pc}^{-3}$ with $\rho_{0.002} \sim 1$. The mean DM mass density is $\rho_{\text{dm}} \simeq 3.6 \times 10^{10}M_\odot \text{ Mpc}^{-3}$ [110] and so the rate per unit comoving volume in the Universe is

$$\Gamma \simeq 1.1 \times 10^{-4}\rho_{0.002}v_{\text{pbh}-200}^{-11/7}\text{Gpc}^{-3}\text{yr}^{-1}. \quad (65)$$

The LIGO collaboration estimated a range of merger rate between $2-53 \text{ Gpc}^{-3}\text{yr}^{-1}$ [112]. This is considerably larger than the estimated rate in Eq. 65.

The above calculation is a very rough estimate. It was assumed that all DM resides in Milky-Way like halos, but a more detailed calculation using a halo mass function would provide a better estimate. The difficulty is that below the mass of the dwarf galaxies we do not know this mass function anymore. For this reason the signal from halos with $M < 400M_\odot$ should be neglected. This way, the total merger rate was estimated to be [110]

$$\mathcal{V} \simeq 2f_{\text{pbh}}^{53/21}\text{Gpc}^{-3}\text{yr}^{-1}, \quad (66)$$

where f_{pbh} is the fraction of DM that consists of PBHs. If all DM consists of PBHs, i.e. $f_{\text{pbh}} = 1$, this estimate is compatible with the LIGO rate in order of magnitude.

4.3.3 PBH binary formation in the early Universe

Besides the formation of PBH binaries from close encounters in the Universe today, there is also a possibility that PBH binaries formed in the early Universe. The MACHO collaboration [113] suggested that in the standard spherical flat rotation halo model $0.62^{+0.3}_{-0.2}$ of the halo consists of massive astrophysical compact halo objects (MACHOs) of mass $\sim 0.5M_\odot$. These MACHOs could in principle be any astrophysical bodies. Nakamura et al. [114] suggested that black hole MACHOs (BHMACHOs) could explain the presence of DM in galaxy halos. They considered the formation of solar mass black holes in the very early Universe. Sasaki et al. [115] adopted this formation scenario but applied it PBHs of mass $\sim 30M_\odot$ and considered the fraction of PBHs in dark matter a free parameter.

The general idea is as follows. If two near PBHs have a sufficiently small separation they form a binary in the early Universe and coalesce within the age of the Universe [115]. The physical mean separation \bar{x} of BHs at matter-radiation equality (redshift z_{eq}) is given by

$$\bar{x} = \left(\frac{M_{\text{BH}}}{\rho_{\text{BH}}(z_{\text{eq}})} \right)^{1/3}, \quad (67)$$

where M_{BH} is the BH mass and ρ_{BH} is BH density. Consider a pair of BHs separated by a distance x at matter-radiation equality. The pair decouples from the expansion of the Universe and forms a stable binary when the average energy density of the BHs exceeds the background cosmic energy density ρ :

$$M_{\text{BH}}R^{-3} > \rho(z), \quad (68)$$

where R is the separation of two BHs. Using $R = \frac{1+z_{\text{eq}}}{1+z}x$ and Eq. 67, it can be shown that [115]

$$f \left(\frac{\bar{x}}{x} \right)^3 - 1 > 0, \quad (69)$$

where f is the fraction of PBHs in DM. From this it follows that only pairs having $x < f^{1/3}\bar{x}$ can form binaries. If there are only two BHs in this scenario, they move closer together and collide without forming a binary [115]. But other BHs are also present and a third BH could affect the infall motion via a tidal force. The major and minor axes of the binary (a, b) are given by

$$a = \frac{\alpha}{f} \frac{x^4}{\bar{x}^3}, \quad b = \beta \left(\frac{x}{y} \right) a, \quad (70)$$

where y is the physical distance to the third BH and α, β are numerical factors. Using the condition $x < f^{1/3}\bar{x}$, the probability that such binaries coalesce in a certain time interval can be calculated. From there the merger rate as a function of the fraction f can be estimated, as shown in figure 15.

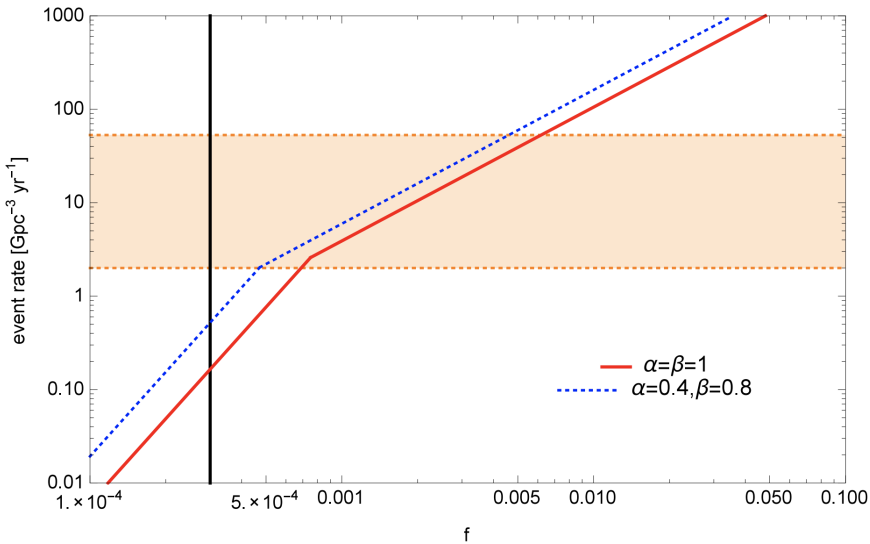


Figure 15: Event rate of mergers of $30M_{\odot} - 30M_{\odot}$ PBH binaries as a function of the PBH fraction in dark matter $f = \Omega_{\text{BH}}/\Omega_{\text{DM}}$. The red line is the case for $\alpha = \beta = 1$, the blue dotted line is the case for $\alpha = 0.4, \beta = 0.8$. The event rate estimated by the LIGO-Virgo Collaboration is shown as the shaded region colored orange. The black solid line at $f \sim 3 \times 10^{-4}$ is the upper limit on f from the nondetection of the CMB spectral distortion obtained in [116]. Figure taken from [115].

Sasaki et al. found that the merger rate falls in the LIGO range of $2 - 53$ $\text{Gpc}^{-3} \text{yr}^{-1}$ if the fraction f is around 10^{-1} [115]. They conclude that the gravitational wave event GW150914 measured by LIGO could be a PBH binary merger, but they ignored the effects of cosmological evolution in their analysis. Ali-Haïmoud et al. [6] recalculated the merger rate of PBH binaries accounting for tidal torquing by all other PBHs, as well as standard large-scale adiabatic perturbations. The result is shown in figure 16. The predicted merger rate would exceed the upper bound from LIGO greatly if PBHs make up all DM. Ali-Haïmoud et al. constrained the abundance of PBHs to be less than 1% of the DM [6].

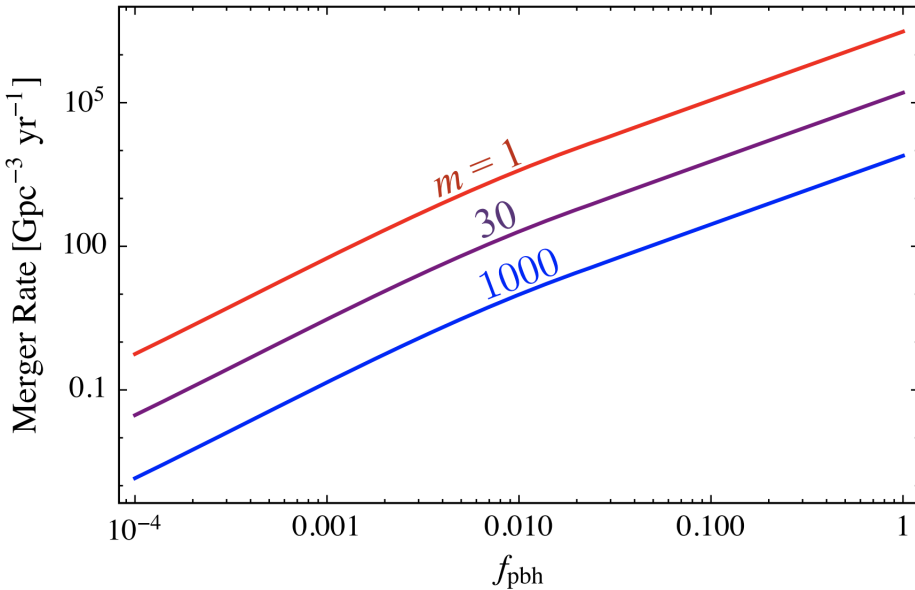


Figure 16: PBH binary merger rate, as a function of PBH fraction f_{pbh} and mass $m = M/M_\odot$. Figure taken from [6].

4.4 Gravitational lensing (Samuel)

The best way to study dark matter is via gravitational influences on ordinary detectable matter [117], as dark matter (almost) exclusively interacts gravitationally. The most direct method for this, is called *gravitational lensing*. In the presence of a gravitational field, space-time is warped by which photons are deflected [118]. The mass that causes the gravitational field acts a lens that bends the path of a photon. This effect was first discovered in 1919, during a solar eclipse in front of the Hyades cluster. The stars in this cluster appeared to move as they passed behind the sun [119]. At first, this observed effect was an experimental verification for Einstein's theory of general relativity. However, gravitational lensing currently is a useful method to probe dark matter. Lensing observations already contributed to several important features for dark matter [117], in agreement with other types of dark matter probes:

- Dark matter is approximately five times more abundant than ordinary, baryonic matter
- Gravitational interactions of dark matter particles are similar to normal matter gravitational interactions
- The electroweak and self-interaction cross-section is very small
- Dark matter is non-relativistic

There are different types of gravitational lensing that can be distinguished: strong lensing, microlensing, weak lensing and femtolensing. These types will be explained below and the most important results of lensing observations regarding dark matter are discussed.

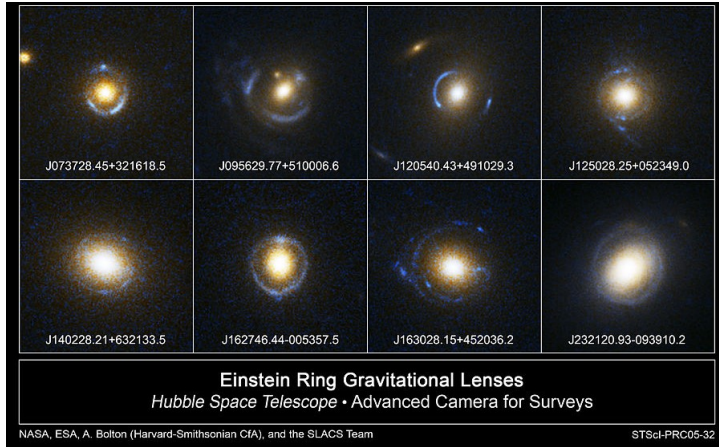


Figure 17: Einstein rings observed by the Hubble Space Telescope. Photons are deflected around a circle-like massive object to form a ring.

4.4.1 Strong lensing

In case of strong gravitational lensing, space-time is warped such that photons can travel along multiple paths around the lens and eventually still be deflected back towards the observer [120]. Photons coming from distant sources directly behind a circular lens can travel around any side of this lens and may form an Einstein ring, see Figure 17. The radius of the Einstein ring is proportional to the square root of the projected mass inside the ring. In case the lens is not circular shape, yet has a complex shape, the photon source may still be appearing at multiple locations, observed at slightly different angles [117]. The first strong gravitational lens that was found was discovered in 1979 with the Jodrell Bank MkIA radio telescope [121]. The lens consists of two quasars, 6 arcseconds apart, with similar redshifts of around 1.41 and absorption spectra.

4.4.2 Microlensing

Observations on distant astronomical bodies are often static on a human lifetime scale. However, this is not the case if there is a relative motion between the photon source and a gravitational lens [117]. The line of sight to a star, of which the photons are bent due to a gravitational lens, represents a volume of space. Currently, advanced panoramic imaging cameras are able to monitor the line of sights to millions of stars. An object that traverses any of the volumes represented by these lines, may brighten the volumes. It is important that the fluctuations in detected brightness are distinguished from the intrinsic fluctuations of the photon source in order to determine the presence of a lens. With this method it is possible to locate dark matter, where the invisible dark matter plays the role of a gravitational lens passing by. One conclusion that was derived from microlensing observations is that dark matter in the Milky Way is not in the form of planet-sized, freefloating clumps, yet these planet-sized clumps do exist in the neighborhood of stars. These dark matter bodies cause secondary brightness peaks shortly before or after their corresponding star itself acts as a gravitational lens [117].

Microlensing applies to relatively small galactic sources as larger sources, like galaxies, are effectively immune to this effect. Only a small fraction of the photons

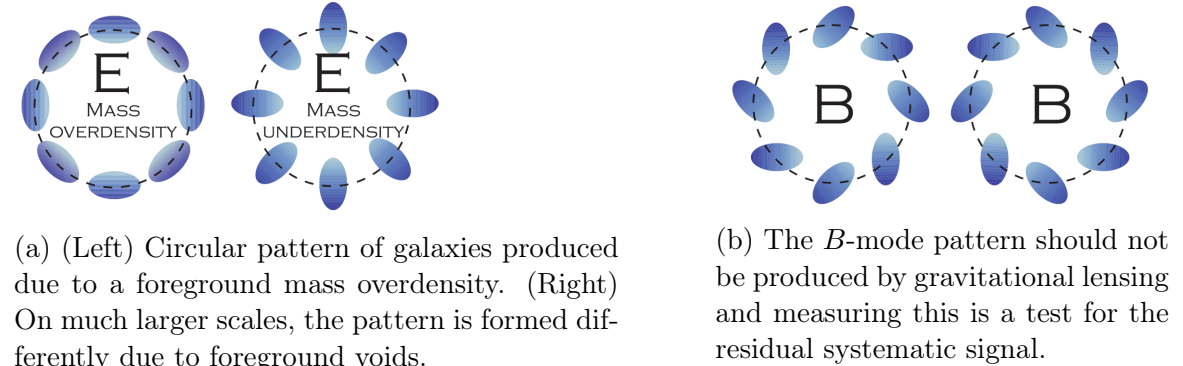


Figure 18: E-mode and B-mode patterns [117]

coming from large sized sources is bent, while the larger part of the photons travels through space of which their paths are not significantly bent.

Detection of PBHs is best possible via microlensing [122]. The M31 surveys monitored stars over the whole galactic disk and bulge and therefore probe a relatively large fraction of the Andromeda dark matter halo. In the research, 56 microlensing events were detected in M31 with large varying time-ranges, from a few to hundred days. The microlensing effect was not due to fluctuations of the photon source, indicating the possible presence of PBHs [122]. Results based on the study of [122] on most likely estimates for PBHs are masses of 0.5-1.0 or 0.05-0.45 solar masses.

A more than 5 years during study in the Large Magellanic Cloud on 11.9 million stars resulted in 13-17 events of microlensing [123]. It ruled out that MACHOs, as PBHs, could not make up all the dark matter on a 95% confidence level. Furthermore, the most likely mass for MACHOs is between 0.15 and 0.9 solar masses.

4.4.3 Weak lensing

Most lines of sight to photon sources do not travel close to a strong gravitational lens [117]. Photons are thus often deflected slightly. In the *weak lensing* regime, the distortion of the photon paths can be approximated as a locally linear transformation of the sky. This transformation can be represented as a 2×2 matrix, with magnification on the diagonal elements and shear as the off-diagonal elements. All elements of the matrix can be measured [124]. The observed shear is proportional to a second derivative of the gravitational potential projected along a line of sight, which is used to determine the projected mass distribution. The mass is a different second derivative of the potential and causes circular patterns (*E-mode*). Figure 18a shows the circular *E-mode* pattern. A shear field, a so-called *B-mode* (see Figure 18b), should not be produced by the gravitational field of a single mass distribution [117]. However, *E* and *B*-modes are equally produced by many different potential systematics. This implies that the *B*-mode consistent with zero should provide a proper test that a sky analysis is successfully cleared of any residual instrumental systematics.

By means of weak lensing, the large scale structure of the sky can be mapped. The light of galaxies is bent slightly due to the large scale dark matter structure. This causes the galaxies to have different observed shapes through different parts of the universe. For a large number of galaxies, the average ellipticity of a subset of these galaxies is determined and mapped (see Figure 19).

4.4.4 Femtolensing

A promising method for probing primordial black holes is considering femtolensing observations [125]. The Schwarzschild radius of primordial black holes is of the same order of the photon wavelength. Consequently, the wave behavior of EM radiation is of importance. As a result, the PBHs cause an interferometry pattern in the energy spectrum of the object from which the photons are deflected. The angular distance between the lensed images is very small and therefore it is called the femtolensing effect. Observations resulted in constraints on the mass range for PBHs. Femtolensing improved the already constrained range of $5 \times 10^{17} - 10^{20}$ grams [125].

4.4.5 More results for dark matter

Using gravitational lensing observations, numerous features of dark matter can be probed. Some examples are the amount of dark matter in the universe or the dark matter abundance in one single galaxy. One obtained result is that haloes of approximately $1.2 \times 10^{13} M_{\odot}$ were found around elliptical galaxies that have a stellar mass of around $2.6 \times 10^{11} M_{\odot}$ [126]. Furthermore, elliptical galaxies contain two times more dark matter haloes than spiral galaxies with similar stellar mass [127]. Other interesting quantities to investigate by means of gravitational lensing are the dark matter distribution ranging from small to large scale structures, and the interactions of dark matter particles [117].

4.5 Constraints from X-ray / Radio (Davey)

As normal black holes accrete matter, PBHs are expected to accrete matter as well. This matter then forms an accretion disk, in which particles will slow down due to friction and fall inward to the PBH. As they fall, they heat up, emitting electromagnetic radiation. Thus, if there are any primordial black holes in our galaxy massive enough to accrete mass, we should be able to detect the radiation emitted from the accretion disk.

Thanks to the gravitational wave detection of a binary black hole system by LIGO/VIRGO, interest was again found for PBHs, as the masses of these binaries were $\approx 30 M_{\odot}$, which is unexpectedly high for normal black holes. If instead these binaries were primordial black holes and thus not created in stellar collapse, then there would need to be $\mathcal{O}(10^9)$ PBHs within 2 kpc from the center of our galaxy for PBHs to constitute all dark matter in that region. As the density of interstellar gas is high near the galactic center, this means that at least some of these PBHs will accrete interstellar gas and thus produce radiation. Studying x-ray and radio sources within our galaxy can then provide useful insights into a possible population of PBHs in the Milky Way. As research in this area is still very fresh, not many groups have tried to find or constrain PBHs using this method. In this section, the most notable result within this area of research, namely that of Gaggero et al.(2017)[128], will be reviewed, followed by a short discussion of the ongoing debate within this subject.

To start, the bolometric luminosity for an accreting black hole is given by $L_B = \eta \dot{M} c^2$, where η is the radiative efficiency, $\eta = 0.1 \dot{M} / (M_{crit})$. Taking PBHs to be inefficient accretors, their luminosity will scale with their accretion rate as $L \propto \dot{M}^2$.

Parametrizing the accretion rate as $\dot{M} = \lambda \dot{M}_{\text{Bondi}}$, where \dot{M}_{Bondi} is the Bondi-Hoyle-Lyttleton accretion rate[107], the accretion rate of a black hole becomes

$$\dot{M} = 4\pi\lambda(GM_{BH})^2\rho(v_{BH}^2 + c_s^2)^{-3/2}, \quad (71)$$

with G the gravitational constant, M_{BH} the mass of the black hole, ρ the density of the accretion disk, v_{BH} the velocity of the black hole and c_s the speed of sound in the accreted material. Using the approximation $L_X \approx 0.3L_B$ for the luminosity of an accreting black hole in the X-ray band and using the relation between X-ray and radio emission discussed in [129], Gaggero et al.[128] calculated the expected X-ray and radio luminosity for a population of PBHs and compared these to galactic surveys and catalogs. From this an upper limit was found on the fractional density of primordial black holes with respect to the dark matter density, which is shown in fig 20. This means that in the mass range of the black holes detected by LIGO, $\mathcal{O}(10) M_\odot$, PBHs cannot make up more than 10% of the total dark matter density.

As this area of research is still very new, this result sparked somewhat of a debate. In [130] the same methodology was used as in [128], but with different assumptions regarding gas turbulence within the accretion region and the density profile of dark matter, resulting in a lower PBH luminosity. From this it was claimed that PBHs cannot be ruled out yet by current X-ray surveys. While x-ray and radio emission seems to be a promising area of PBH research, it remains to be seen whether this has already ruled them out as a dark matter candidate. Future experiments like the Square Kilometre Array(SKA) will hopefully be able to provide definite answers, and until then the debate will continue.

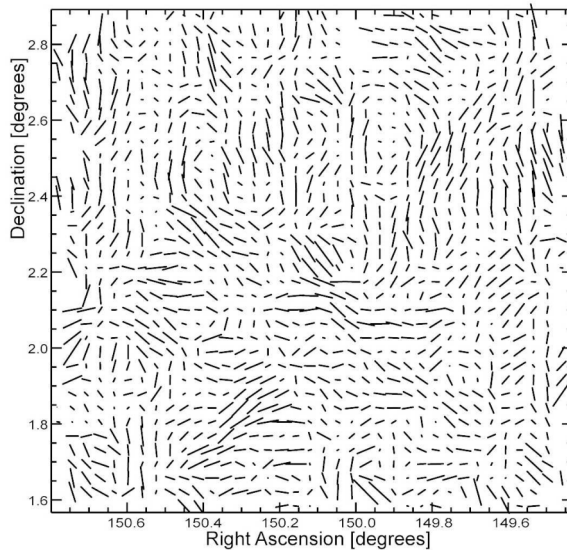


Figure 19: Observed ellipticities for 0.5 million galaxies in the 2 squared degree Hubble Space Telescope COSMOS survey. Each dash represents the magnitude and direction of the ellipticity of several hundred galaxies. The longer the dash, the more elliptic, in proportion to the semi-major axis of the galaxy. [117].

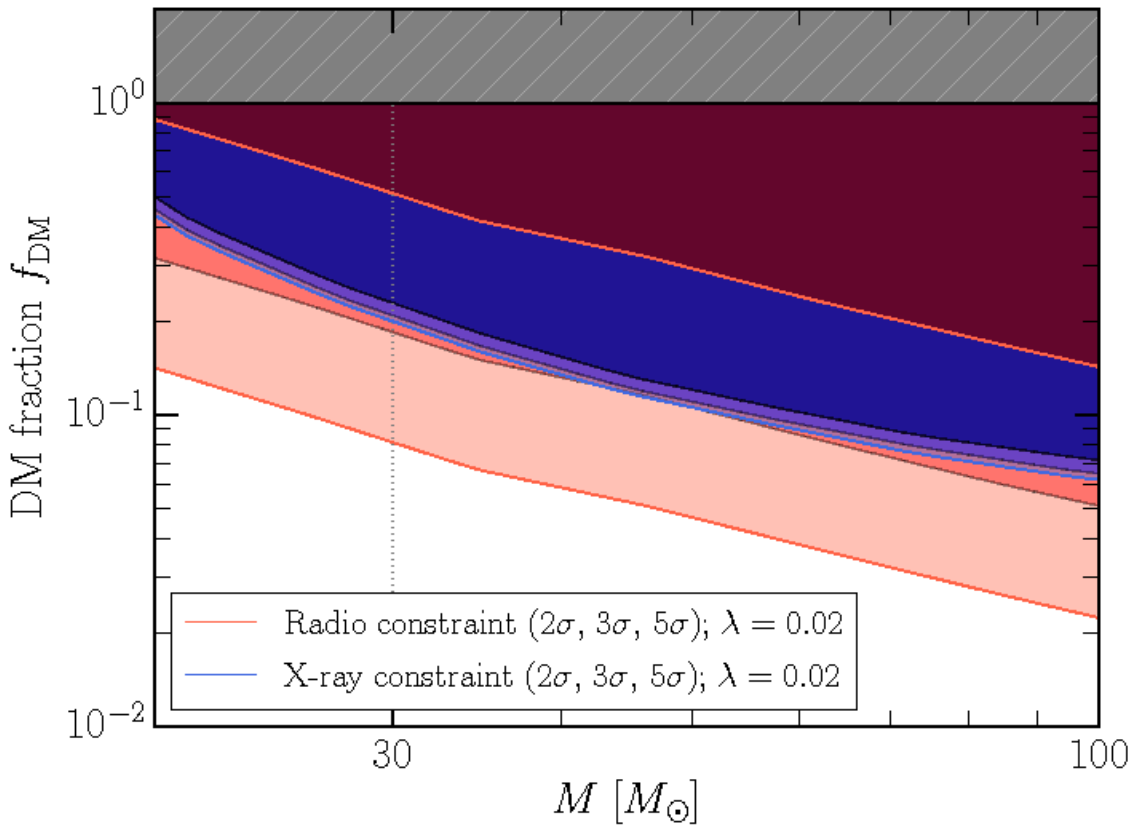


Figure 20: Upper limits on the fraction of dark matter in PBHs of mass M , from the X-ray (blue) and radio (red) regimes at the galactic center. The dotted grey line corresponds to $30M_{\odot}$ PBH.

References

- [1] Leszek Roszkowski, Enrico Maria Sessolo, and Sebastian Trojanowski. WIMP dark matter candidates and searches - current status and future prospects. *Rept. Prog. Phys.*, 81(6):066201, 2018.
- [2] Gianfranco Bertone, Nassim Bozorgnia, Jong Soo Kim, Sebastian Liem, Christopher McCabe, Sydney Otten, and Roberto Ruiz de Austri. Identifying WIMP dark matter from particle and astroparticle data. *JCAP*, 1803(03):026, 2018.
- [3] Maxim Yu Khlopov. Probes for Dark Matter Physics. *Int. J. Mod. Phys.*, D27(06):1841013, 2018.
- [4] David G. Cerdeno. WIMPs: A brief bestiary. In *Proceedings, 4th Patras Workshop on Axions, WIMPs and WISPs (AXION-WIMP 2008): Hamburg, Germany, June 18-21, 2008*, pages 9–12, 2009.
- [5] B. P. Abbott et al. Observation of Gravitational Waves from a Binary Black Hole Merger. *Phys. Rev. Lett.*, 116(6):061102, 2016.
- [6] Yacine Ali-Haimoud, Ely D. Kovetz, and Marc Kamionkowski. Merger rate of primordial black-hole binaries. *Phys. Rev.*, D96(12):123523, 2017.
- [7] Gerard Jungman, Marc Kamionkowski, and Kim Griest. Supersymmetric dark matter. *Phys. Rept.*, 267:195–373, 1996.
- [8] George R. Blumenthal, Heinz Pagels, and Joel R. Primack. GALAXY FORMATION BY DISSIPATIONLESS PARTICLES HEAVIER THAN NEUTRINOS. *Nature*, 299:37–38, 1982.
- [9] P. Kroupa, B. Famaey, K. S. de Boer, J. Dabringhausen, M. S. Pawłowski, C. M. Boily, H. Jerjen, D. Forbes, G. Hensler, and M. Metz. Local-Group tests of dark-matter Concordance Cosmology: Towards a new paradigm for structure formation? *Astron. Astrophys.*, 523:A32, 2010.
- [10] Scott Burles, Kenneth M. Nollett, and Michael S. Turner. Big bang nucleosynthesis predictions for precision cosmology. *Astrophys. J.*, 552:L1–L6, 2001.
- [11] David Kirkman, David Tytler, Nao Suzuki, John M. O’Meara, and Dan Lubin. The Cosmological baryon density from the deuterium to hydrogen ratio towards QSO absorption systems: D/H towards Q1243+3047. *Astrophys. J. Suppl.*, 149:1, 2003.
- [12] Paolo Gondolo. Non-baryonic dark matter. *NATO Sci. Ser. II*, 187:279–333, 2005. [,279(2003)].
- [13] *Supersymmetry, Part I (Theory), Revised by Howard E. Haber* , 2013. <http://pdg.lbl.gov/2014/reviews/rpp2014-rev-susy-1-theory.pdf>.
- [14] N. Arkani-Hamed, A. G. Cohen, E. Katz, and A. E. Nelson. The Littlest Higgs. *JHEP*, 07:034, 2002.

-
- [15] Stefano Profumo. Astrophysical Probes of Dark Matter. In *Proceedings, Theoretical Advanced Study Institute in Elementary Particle Physics: Searching for New Physics at Small and Large Scales (TASI 2012): Boulder, Colorado, June 4-29, 2012*, pages 143–189, 2013.
- [16] Scott Dodelson. *Modern Cosmology*. Academic Press, Amsterdam, 2003.
- [17] Graciela Gelmini and Paolo Gondolo. DM Production Mechanisms. pages 121–141, 2010.
- [18] Benjamin W. Lee and Steven Weinberg. Cosmological Lower Bound on Heavy Neutrino Masses. *Phys. Rev. Lett.*, 39:165–168, 1977. [,183(1977)].
- [19] Kim Griest and Marc Kamionkowski. Unitarity Limits on the Mass and Radius of Dark Matter Particles. *Phys. Rev. Lett.*, 64:615, 1990.
- [20] Gary Steigman, Basudeb Dasgupta, and John F. Beacom. Precise Relic WIMP Abundance and its Impact on Searches for Dark Matter Annihilation. *Phys. Rev.*, D86:023506, 2012.
- [21] Nir Polonsky. Supersymmetry: Structure and phenomena. Extensions of the standard model. *Lect. Notes Phys. Monogr.*, 68:1–169, 2001.
- [22] H. E. Haber and Gordon L. Kane. The search for supersymmetry: Probing physics beyond the standard model. *Physics Reports*, 117 (2-4):75–263, 1985.
- [23] Mohammad Abdullah and Jonathan L. Feng. Reviving bino dark matter with vectorlike fourth generation particles. *Phys. Rev.*, D93(1):015006, 2016.
- [24] Gerard Jungman, Marc Kamionkowski, and Kim Griest. Supersymmetric dark matter. *Physics Reports*, 267(5):195 – 373, 1996.
- [25] Kim Griest, Marc Kamionkowski, and Michael S. Turner. Supersymmetric dark matter above the w mass. *Phys. Rev. D*, 41:3565–3582, Jun 1990.
- [26] K. Becker, M. Becker, and J. H. Schwarz. *String theory and M-theory: A modern introduction*. Cambridge University Press, 2006.
- [27] Gianfranco Bertone, Dan Hooper, and Joseph Silk. Particle dark matter: Evidence, candidates and constraints. *Phys. Rept.*, 405:279–390, 2005.
- [28] Thomas Appelquist, Hsin-Chia Cheng, and Bogdan A. Dobrescu. Bounds on universal extra dimensions. *Phys. Rev.*, D64:035002, 2001.
- [29] Nima Arkani-Hamed, Savas Dimopoulos, and G. R. Dvali. The Hierarchy problem and new dimensions at a millimeter. *Phys. Lett.*, B429:263–272, 1998.
- [30] Bogdan A. Dobrescu and Erich Poppitz. Number of fermion generations derived from anomaly cancellation. *Phys. Rev. Lett.*, 87:031801, 2001.
- [31] Lisa Randall and Raman Sundrum. An Alternative to compactification. *Phys. Rev. Lett.*, 83:4690–4693, 1999.

- [32] Avirup Shaw. KK-parity non-conservation in UED confronts LHC data. *Eur. Phys. J.*, C75(1):33, 2015.
- [33] Geraldine Servant and Timothy M. P. Tait. Is the lightest Kaluza-Klein particle a viable dark matter candidate? *Nucl. Phys.*, B650:391–419, 2003.
- [34] Edward W. Kolb and Richard Slansky. Dimensional Reduction in the Early Universe: Where Have the Massive Particles Gone? *Phys. Lett.*, 135B:378, 1984.
- [35] David Tong. String Theory. 2009.
- [36] Hsin-Chia Cheng, Konstantin T. Matchev, and Martin Schmaltz. Radiative corrections to Kaluza-Klein masses. *Phys. Rev.*, D66:036005, 2002.
- [37] Geraldine Servant and Timothy M. P. Tait. Elastic scattering and direct detection of Kaluza-Klein dark matter. *New J. Phys.*, 4:99, 2002.
- [38] D. J. Kapner, T. S. Cook, E. G. Adelberger, J. H. Gundlach, Blayne R. Heckel, C. D. Hoyle, and H. E. Swanson. Tests of the gravitational inverse-square law below the dark-energy length scale. *Phys. Rev. Lett.*, 98:021101, 2007.
- [39] Felix Kahlhoefer. Review of LHC Dark Matter Searches. *Int. J. Mod. Phys.*, A32(13):1730006, 2017.
- [40] Philip Bechtle et al. Killing the cMSSM softly. *Eur. Phys. J.*, C76(2):96, 2016.
- [41] Georges Aad et al. Summary of the ATLAS experiment’s sensitivity to supersymmetry after LHC Run 1 — interpreted in the phenomenological MSSM. *JHEP*, 10:134, 2015.
- [42] ATLAS Collaboration. Summary plots from the ATLAS Exotic physics group. <https://atlas.web.cern.ch/Atlas/GROUPS/PHYSICS/CombinedSummaryPlots/EXOTICS/index.html>, 2017.
- [43] Q. R. Ahmad et al. Direct evidence for neutrino flavor transformation from neutral current interactions in the Sudbury Neutrino Observatory. *Phys. Rev. Lett.*, 89:011301, 2002.
- [44] Y. Fukuda et al. Evidence for oscillation of atmospheric neutrinos. *Phys. Rev. Lett.*, 81:1562–1567, 1998.
- [45] Alexey Boyarsky, Dmytro Iakubovskyi, and Oleg Ruchayskiy. Next decade of sterile neutrino studies. *Phys. Dark Univ.*, 1:136–154, 2012.
- [46] C. Patrignani et al. Review of Particle Physics. *Chin. Phys.*, C40(10):100001, 2016.
- [47] E. Komatsu et al. Seven-Year Wilkinson Microwave Anisotropy Probe (WMAP) Observations: Cosmological Interpretation. *Astrophys. J. Suppl.*, 192:18, 2011.
- [48] S. Tremaine and J. E. Gunn. Dynamical Role of Light Neutral Leptons in Cosmology. *Phys. Rev. Lett.*, 42:407–410, 1979. [,66(1979)].

- [49] Scott Dodelson and Lawrence M. Widrow. Sterile-neutrinos as dark matter. *Phys. Rev. Lett.*, 72:17–20, 1994.
- [50] Takehiko Asaka and Mikhail Shaposhnikov. The nuMSM, dark matter and baryon asymmetry of the universe. *Phys. Lett.*, B620:17–26, 2005.
- [51] M. Drewes et al. A White Paper on keV Sterile Neutrino Dark Matter. *JCAP*, 1701(01):025, 2017.
- [52] Alexey Boyarsky, Oleg Ruchayskiy, and Mikhail Shaposhnikov. The Role of sterile neutrinos in cosmology and astrophysics. *Ann. Rev. Nucl. Part. Sci.*, 59:191–214, 2009.
- [53] A. Yu. Smirnov. The MSW effect and solar neutrinos. In *Neutrino telescopes. Proceedings, 10th International Workshop, Venice, Italy, March 11-14, 2003. Vol. 1+2*, pages 23–43, 2003.
- [54] Alexey Boyarsky, Julien Lesgourgues, Oleg Ruchayskiy, and Matteo Viel. Realistic sterile neutrino dark matter with keV mass does not contradict cosmological bounds. *Phys. Rev. Lett.*, 102:201304, 2009.
- [55] Dmitry Gorbunov and Mikhail Shaposhnikov. How to find neutral leptons of the ν MSM? *JHEP*, 10:015, 2007. [Erratum: JHEP11,101(2013)].
- [56] R. E. Shrock. New Tests For, and Bounds On, Neutrino Masses and Lepton Mixing. *Phys. Lett.*, 96B:159–164, 1980.
- [57] Steven Weinberg. A new light boson? *Phys. Rev. Lett.*, 40:223–226, Jan 1978.
- [58] Leanne D Duffy and Karl van Bibber. Axions as dark matter particles. *New Journal of Physics*, 11(10):105008, 2009.
- [59] P. Schmidt-Wellenburg. The quest to find an electric dipole moment of the neutron. 2016.
- [60] R. D. Peccei. The Strong CP problem and axions. *Lect. Notes Phys.*, 741:3–17, 2008. [,3(2006)].
- [61] Tom Banks and Michael Dine. The cosmology of string theoretic axions. *Nuclear Physics B*, 505(1):445 – 460, 1997.
- [62] Pierre Sikivie. Axion Cosmology. *Lect. Notes Phys.*, 741:19–50, 2008. [,19(2006)].
- [63] David J. Gross, Robert D. Pisarski, and Laurence G. Yaffe. Qcd and instantons at finite temperature. *Rev. Mod. Phys.*, 53:43–80, Jan 1981.
- [64] K. Zioutas, M. Tsagri, Y. Semertzidis, T. Papaevangelou, T. Dafni, and Anastassopoulos V. Axion searches with helioscopes and astrophysical signatures for axion(-like) particles. *New Journal of Physics*, 11, 2009.
- [65] P. Sikivie. Experimental tests of the "invisible" axion. *Phys. Rev. Lett.*, 51:1415–1417, Oct 1983.

-
- [66] P. Sikivie. Detection rates for “invisible”-axion searches. *Phys. Rev. D*, 32:2988–2991, Dec 1985.
- [67] V. Anastassopoulos et al. New CAST Limit on the Axion-Photon Interaction. *Nature Phys.*, 13:584–590, 2017.
- [68] T. Dafni and Francisco Jose Iguaz. Axion helioscopes update: the status of CAST & IAXO. *PoS*, TIPP2014:130, 2014.
- [69] Dmitry Lyapustin. The axion dark matter experiment. *Physics in Collision*, 1, 2011.
- [70] J. Beringer et al. Review of Particle Physics (RPP). *Phys. Rev.*, D86:010001, 2012.
- [71] J. K. Vogel et al. IAXO - The International Axion Observatory. In *8th Patras Workshop on Axions, WIMPs and WISPs (AXION-WIMP 2012) Chicago, Illinois, July 18-22, 2012*, 2013.
- [72] Lam Hui, Jeremiah P. Ostriker, Scott Tremaine, and Edward Witten. Ultralight scalars as cosmological dark matter. *Phys. Rev.*, D95(4):043541, 2017.
- [73] David H. Weinberg, James S. Bullock, Fabio Governato, Rachel Kuzio de Naray, and Annika H. G. Peter. Cold dark matter: controversies on small scales. *Proc. Nat. Acad. Sci.*, 112:12249–12255, 2015.
- [74] Paul Bode, Jeremiah P. Ostriker, and Neil Turok. Halo formation in warm dark matter models. *Astrophys. J.*, 556:93–107, 2001.
- [75] Asimina Arvanitaki, Savas Dimopoulos, Sergei Dubovsky, Nemanja Kaloper, and John March-Russell. String Axiverse. *Phys. Rev.*, D81:123530, 2010.
- [76] Shamit Kachru, Renata Kallosh, Andrei D. Linde, Juan Martin Maldacena, Liam P. McAllister, and Sandip P. Trivedi. Towards inflation in string theory. *JCAP*, 0310:013, 2003.
- [77] JoAnne L. Hewett and Thomas G. Rizzo. Low-Energy Phenomenology of Superstring Inspired E(6) Models. *Phys. Rept.*, 183:193, 1989.
- [78] Kiwoon Choi and Jihn E. Kim. Compactification and Axions in E(8) x E(8)-prime Superstring Models. *Phys. Lett.*, 165B:71–75, 1985.
- [79] Peter Svrcek and Edward Witten. Axions In String Theory. *JHEP*, 06:051, 2006.
- [80] Renée Hlozek, Daniel Grin, David J. E. Marsh, and Pedro G. Ferreira. A search for ultralight axions using precision cosmological data. *Phys. Rev.*, D91(10):103512, 2015.
- [81] D. N. Spergel et al. Wilkinson Microwave Anisotropy Probe (WMAP) three year results: implications for cosmology. *Astrophys. J. Suppl.*, 170:377, 2007.

-
- [82] Volker Bromm, Paolo S. Coppi, and Richard B. Larson. The formation of the first stars. I. The Primordial star forming cloud. *Astrophys. J.*, 564:23–51, 2002.
- [83] Wayne Hu, Rennan Barkana, and Andrei Gruzinov. Cold and fuzzy dark matter. *Phys. Rev. Lett.*, 85:1158–1161, 2000.
- [84] Shu-Rong Chen, Hsi-Yu Schive, and Tzihong Chiueh. Jeans Analysis for Dwarf Spheroidal Galaxies in Wave Dark Matter. *Mon. Not. Roy. Astron. Soc.*, 468(2):1338–1348, 2017.
- [85] Keisuke Harigaya, Tongyan Lin, and Hou Keong Lou. GUTzilla Dark Matter. *JHEP*, 09:014, 2016.
- [86] Daniel J. H. Chung, Edward W. Kolb, and Antonio Riotto. Production of massive particles during reheating. *Phys. Rev.*, D60:063504, 1999.
- [87] Edward W. Kolb, Daniel J. H. Chung, and Antonio Riotto. WIMPzillas! *AIP Conf. Proc.*, 484(1):91–105, 1999. [,592(1999)].
- [88] Daniel J. H. Chung, Patrick Crotty, Edward W. Kolb, and Antonio Riotto. On the gravitational production of superheavy dark matter. *Phys. Rev.*, D64:043503, 2001.
- [89] Edward W. Kolb, A. A. Starobinsky, and I. I. Tkachev. Trans-Planckian wimpzillas. *JCAP*, 0707:005, 2007.
- [90] Chiaki Hikage, Kazuya Koyama, Takahiko Matsubara, Tomo Takahashi, and Masahide Yamaguchi. Limits on Isocurvature Perturbations from Non-Gaussianity in WMAP Temperature Anisotropy. *Mon. Not. Roy. Astron. Soc.*, 398:2188–2198, 2009.
- [91] Daniel J. H. Chung and Hojin Yoo. Isocurvature Perturbations and Non-Gaussianity of Gravitationally Produced Nonthermal Dark Matter. *Phys. Rev.*, D87:023516, 2013.
- [92] Sanghyeon Chang, Claudio Coriano, and Alon E. Faraggi. Stable superstring relics. *Nucl. Phys.*, B477:65–104, 1996.
- [93] Claudio Coriano, Alon E. Faraggi, and Michael Plumacher. Stable superstring relics and ultrahigh-energy cosmic rays. *Nucl. Phys.*, B614:233–253, 2001.
- [94] Alexander Aab et al. Inferences on mass composition and tests of hadronic interactions from 0.3 to 100 EeV using the water-Cherenkov detectors of the Pierre Auger Observatory. *Phys. Rev.*, D96(12):122003, 2017.
- [95] Bernard J. Carr and S. W. Hawking. Black holes in the early Universe. *Mon. Not. Roy. Astron. Soc.*, 168:399–415, 1974.
- [96] Naresh Dadhich, Roy Maartens, Philippos Papadopoulos, and Vahid Rezania. Black holes on the brane. *Phys. Lett.*, B487:1–6, 2000.
- [97] S. W. Hawking. Black Holes and Thermodynamics. *Phys. Rev.*, D13:191–197, 1976.

- [98] John D. Barrow, Edmund J. Copeland, and Andrew R. Liddle. The Cosmology of black hole relics. *Phys. Rev.*, D46:645–657, 1992.
- [99] Bernard Carr, Florian Kuhnel, and Marit Sandstad. Primordial Black Holes as Dark Matter. *Phys. Rev.*, D94(8):083504, 2016.
- [100] Juan García-Bellido and Sébastien Clesse. Constraints from microlensing experiments on clustered primordial black holes. *Phys. Dark Univ.*, 19:144–148, 2018.
- [101] Julio F. Navarro, Carlos S. Frenk, and Simon D. M. White. The Structure of cold dark matter halos. *Astrophys. J.*, 462:563–575, 1996.
- [102] Marco Roncadelli, Aldo Treves, and Roberto Turolla. Primordial black holes are again on the limelight. 2009.
- [103] Christopher F. McKee and Eve C. Ostriker. Theory of Star Formation. *Ann. Rev. Astron. Astrophys.*, 45:565–687, 2007.
- [104] Fabio Capela, Maxim Pshirkov, and Peter Tinyakov. Constraints on primordial black holes as dark matter candidates from capture by neutron stars. *Phys. Rev.*, D87(12):123524, 2013.
- [105] J. Binney and S. Tremaine. *Galactic dynamics*. 1987.
- [106] G. Steigman, C. L. Sarazin, H. Quintana, and J. Faulkner. Dynamical interactions and astrophysical effects of stable heavy neutrinos. *Astron. J.*, 83:1050–1061, 1978.
- [107] H. Bondi. On spherically symmetrical accretion. *Mon. Not. Roy. Astron. Soc.*, 112:195, 1952.
- [108] G. F. Chapline. Cosmological effects of primordial black holes. *Nature*, 253:251 EP –, 01 1975.
- [109] Ely D. Kovetz. Probing Primordial-Black-Hole Dark Matter with Gravitational Waves. *Phys. Rev. Lett.*, 119(13):131301, 2017.
- [110] Simeon Bird, Ilias Cholis, Julian B. Munoz, Yacine Ali-Haimoud, Marc Kamionkowski, Ely D. Kovetz, Alvise Raccanelli, and Adam G. Riess. Did LIGO detect dark matter? *Phys. Rev. Lett.*, 116(20):201301, 2016.
- [111] Ely D. Kovetz, Ilias Cholis, Patrick C. Breysse, and Marc Kamionkowski. Black hole mass function from gravitational wave measurements. *Phys. Rev.*, D95(10):103010, 2017.
- [112] B. P. Abbott et al. The Rate of Binary Black Hole Mergers Inferred from Advanced LIGO Observations Surrounding GW150914. *Astrophys. J.*, 833(1):L1, 2016.
- [113] C. Alcock et al. The MACHO project LMC microlensing results from the first two years and the nature of the galactic dark halo. *Astrophys. J.*, 486:697–726, 1997.

- [114] Takashi Nakamura, Misao Sasaki, Takahiro Tanaka, and Kip S. Thorne. Gravitational waves from coalescing black hole MACHO binaries. *Astrophys. J.*, 487:L139–L142, 1997.
- [115] Misao Sasaki, Teruaki Suyama, Takahiro Tanaka, and Shuichiro Yokoyama. Primordial Black Hole Scenario for the Gravitational-Wave Event GW150914. *Phys. Rev. Lett.*, 117(6):061101, 2016.
- [116] Massimo Ricotti, Jeremiah P. Ostriker, and Katherine J. Mack. Effect of Primordial Black Holes on the Cosmic Microwave Background and Cosmological Parameter Estimates. *Astrophys. J.*, 680:829, 2008.
- [117] Richard Massey, Thomas Kitching, and Johan Richard. The dark matter of gravitational lensing. *Rept. Prog. Phys.*, 73:086901, 2010.
- [118] Einstein A. Die grundlage der allgemeinen relativitätstheorie [adp 49, 769 (1916)]. *Annalen der Physik*, 14(1):517–571.
- [119] and and. Ix. a determination of the deflection of light by the sun’s gravitational field, from observations made at the total eclipse of may 29, 1919. *Philosophical Transactions of the Royal Society of London A: Mathematical, Physical and Engineering Sciences*, 220(571-581):291–333, 1920.
- [120] Tommaso Treu. Strong lensing by galaxies. *Annual Review of Astronomy and Astrophysics*, 48(1):87–125, 2010.
- [121] D. Walsh, R. F. Carswell, and R. J. Weymann. 0957 + 561 A, B - Twin quasistellar objects or gravitational lens. *nat*, 279:381–384, May 1979.
- [122] Sébastien Clesse and Juan García-Bellido. Seven Hints for Primordial Black Hole Dark Matter. 2017.
- [123] C. Alcock et al. The MACHO project: Microlensing results from 5.7 years of LMC observations. *Astrophys. J.*, 542:281–307, 2000.
- [124] B. Ménard, R. Scranton, M. Fukugita, and G. Richards. Measuring the galaxy-mass and galaxy-dust correlations through magnification and reddening. *MNRAS*, 405:1025–1039, June 2010.
- [125] A. Barnacka, J.-F. Glicenstein, and R. Moderski. New constraints on primordial black holes abundance from femtolensing of gamma-ray bursts. 86(4):043001, August 2012.
- [126] Raphael Gavazzi, Tommaso Treu, Jason D. Rhodes, Leon Ve Koopmans, Adam S. Bolton, Scott Burles, Richard Massey, and Leonidas A. Moustakas. The Sloan Lens ACS Survey. 4. The mass density profile of early-type galaxies out to 100 effective radii. *Astrophys. J.*, 667:176–190, 2007.
- [127] James E. Taylor, Richard J. Massey, Alexie Leauthaud, Matthew R. George, Jason Rhodes, Thomas D. Kitching, Peter Capak, Richard Ellis, Alexis Finoguenov, Olivier Ilbert, Eric Jullo, Jean-Paul Kneib, Anton M. Koekemoer, Nick Scoville, and Masayuki Tanaka. Measuring the geometry of the universe from weak gravitational lensing behind galaxy groups in the hst cosmo survey. *The Astrophysical Journal*, 749(2):127, 2012.

- [128] Daniele Gaggero, Gianfranco Bertone, Francesca Calore, Riley M. T. Connors, Mark Lovell, Sera Markoff, and Emma Storm. Searching for Primordial Black Holes in the radio and X-ray sky. *Phys. Rev. Lett.*, 118(24):241101, 2017.
- [129] Richard M. Plotkin, Sera Markoff, Brandon C. Kelly, Elmar Körding, and Scott F. Anderson. Using the fundamental plane of black hole activity to distinguish x-ray processes from weakly accreting black holes. *Monthly Notices of the Royal Astronomical Society*, 419(1):267–286, 2012.
- [130] Andi Hektor, Gert Hütsi, and Martti Raidal. Constraints on Primordial Black Hole Dark Matter from Galactic Center X-ray observations. 2018.